Effects of various shielding gases on the welding of ferritic stainless steel using alternative electrode ER308L for railway wagons

MSc RESEARCH

Prepared by

Dhurasha Govender

(2254321)

Submitted to

School of Chemical and Metallurgical Engineering, Faculty of Engineering and the Built Environment, University of the Witwatersrand, Johannesburg.

27 September 2022

DECLARATION

I declare that this dissertation is my own, unaided work. It is being submitted for the Degree of Master of Science in the University of the Witwatersrand, Johannesburg. It has not been submitted before for any degree or examination in any other University.

_____

(Signature of candidate)

_____27th_____day of _____September_____2022_____

ABSTRACT

The 3CR12 ferritic stainless-steel alloy was first developed as a cost-effective alternative to AISI 409 ferritic stainless steel, with good weldability and affordability for mildly corrosive environments. The ferritic stainless-steel is used widely in wagon manufacturing, in which welding of the material, makes up a large portion of the costs relating to welding wire, shielding gases and the time taken to weld. The welding process and consumables are crucial elements in producing quality welds during wagon manufacturing. In South Africa, 3CR12 stainless steel is used in the fabrication of wagon's due to its high strength, excellent impact, corrosion, and abrasion resistance. The welding electrode that is currently used in the welding of wagons is the ER309L welding wire which has proven to be compatible in chemical composition. Aside from the high cost, there are no historical welding problems related to ER309L welding wire, however, companies are looking at various ways to manufacture wagons cost effectively. The aim of this research was to find a material and consumable combination that will decrease the manufacturing costs of the wagons. Welding wire ER308L was found to be a suitable candidate after observation of previous findings. The objectives of this study were to then experiment with various shielding gases and different gas ratios of these gases to obtain optimum weld properties. Eight sets of 3CR12 plates were welded using a different shielding gas ratio per set. The shielding gases contained combinations of argon (Ar), helium (He), oxygen (O_2) and carbon dioxide (CO_2) gases. The experiment entailed the welding and non-destructive inspection of 6 mm thick 3CR12 plates, V- butt welded via gas metal arc welding and laboratory testing including hardness, tensile, Charpy impact and microscopy. It was found that the gas ratios containing, 73% Ar, 2% CO_2, 25% He and, 75% Ar and 25% He respectively, provided the best mechanical and metallurgical results. Impact values in the range of 74 and 99J and yield strengths of 337-362 MPa, were achieved during these tests together with low ferrite content and the absence of sensitisation. Due to a better root penetration of the 73% Ar, 2% CO_2, 25% He gas, it was concluded that this would be the gas recommended to produce wagons as the 75% Ar, 25% He may result in lack of penetration at the root of the weld.

Keywords: Welding 3CR12, ER308L welding wire, wagon manufacturing, various shielding gases.

In memory of my parents

Pat and Kogilan Govender

1956 – 2008

ACKNOWLEDGEMENTS

I would like to express my sincerest gratitude and appreciation to all the people and companies that assisted during this project. In particular, I would like to thank the following individuals -

- God, the Almighty, who has granted countless blessings, knowledge, and opportunity, that have enabled me to finally accomplish this thesis.
- My sisters and brother-in-law for their support and encouragement throughout my career.
- My husband, Shealen Chetty, who has stood by me throughout the duration of my research. Your support, understanding and encouragement has been my strength in achieving this milestone.
- My supervisor, Prof Nthabiseng Maledi for her guidance and support during this research.
- My manager Velaphi Matjeke, for driving and supporting me in accomplishing this milestone.
- My colleagues from Transnet Engineering for all their assistance during the experimental and testing phases of this project.

TABLE OF CONTENTS

LIST OF FIGURES

LIST OF TABLES

LIST OF SYMBOLS

°C	-	degree Celsius
R	-	Rand
wt.%	-	weight percent
vol%	-	volume percent
%	-	percent
α	-	alpha
γ	-	gamma
˚	-	degree
η	-	heat source efficiency
~	-	approximately
bar	-	Metric unit of pressure
kg m^{-3}	-	Unit measurement for density in kilogram per meter cubed
kJ/mm	-	Unit for heat input in kilojoules per millimetre
eV	-	Measurement for ionisation energy in electron volts
MPa	-	Unit measurement of stress in megapascal
J	-	Unit measurement of energy in joule
kgf	-	Unit measurement of load in Kilogram-force

NOMENCLATURE

AISI	-	American Iron and Steel Institute
Ar	-	Argon
ASTM	-	American Society for Testing and Materials
BCC	-	Body-centered cubic is the name given to the type of atom arrangement found in nature.
C	-	Carbon
CO_2	-	Carbon dioxide
Cr	-	Chromium
DBTT	-	Ductile to brittle transition temperature
DC+	-	Direct current positive
DC-	-	Direct current negative
EBW	-	Electron beam welding
FGHAZ	-	Fine grained heat affected zone
FSW	-	Friction-stir welding
GMAW	-	Gas metal arc welding
GTAW	-	Gas tungsten arc welding
HAZ	-	Heat affected zone
He	-	Helium
HTHAZ	-	High temperature heat affected zone
HV	-	Vickers hardness
ISSF	-	International Stainless-Steel Forum
KFF	-	Kaltenhauser ferrite factor
LBW	-	Laser beam welding
LTHAZ	-	Low temperature heat-affected zone
$M_{23}C_6$	-	Chromium carbide
Mn	-	Manganese
Mo	-	Molybdenum
MT	-	Magnetic Particle Testing
O_2	-	Oxygen
N	-	Nitrogen atom
Nb	-	Niobium

NDT	-	Non-destructive Testing
N_2	-	Nitrogen molecule
Ni	-	Nickel
P	-	Phosphorus
$R_p0.2$	-	Yield strength at 0.2% offset or 0.2% proof stress
R_m	-	Ultimate tensile strength
S	-	Sulphur
Si	-	Silicon
Ti	-	Titanium
USA	-	United States of America
UK	-	United Kingdom
VT	-	Visual Testing
WITT	-	A manufacturer of gas-related equipment located in Witten Germany. The family-owned company was founded by Paul Witt in 1945.
XRD	-	X-ray Diffraction

1.CHAPTER 1

1.1. Introduction

Freight rail manufacturers across the world have used various materials to produce wagons. In countries such as Poland, Australia and China, carbon steel has been the material of choice used to produce most freight vehicles primarily due to its affordability. Although mild carbon steel is known to have good weldability and mechanical strength, it is prone to corrosion which increases in material handling applications. As a substitute to the regular carbon steel, South African rail manufacturers previously used the American designed Corten Steel also known as weathered steel (International Stainless-Steel Forum, 2018). Corten Steel was developed specifically to help build railway coal wagons and showed superior corrosion resistance when compared to mild steel. This is due to the protective oxide layer that forms on the surface of Corten Steel which slows down future corrosion. Although exhibiting good corrosion resistance and tensile strength, Corten Steel proved to be difficult to weld due to the formation of defects such as lack of fusion, lack of penetration and porosity (Deepak et al., 2019). The use of Corten steel only lasted about 8 years in South Africa before corrosion problems necessitated rebuilding of wagons. In 1984, South African rail companies began manufacturing wagons using utility (ferritic) steel which exhibited improved corrosion resistance, good strength, better weldability, and lower costs as compared to traditional stainless steel (International Stainless-Steel Forum, 2018). Ferritic steel wagons therefore have a lower life cycle cost compared to mild steel wagons (International Stainless-Steel Forum, 2017).

The previous generation of ferritic stainless steel is known as 3CR12, which was commercialised in South Africa in 1980 (Collen, 2015). It is available from the majority of steel suppliers and conforms to ASTM A240 with UNS S41003 designation, in the United States of America (American Society for Testing and Materials, 2004) and in Europe to Material Number 1.4003 (British Standards Institution, 2014). One of the biggest cost drivers for manufacturing railway vehicles with this stainless steel, however, is the welding operation and consumables. Although 3CR12 has excellent corrosion resistance in many environments, its weldability is limited (Taban, Deleu and Dhooge, 2008). It is for this reason that further research will be conducted for improvement and optimisation of welding 3CR12. The consumable recommended for welding 3CR12 is ER309L, however ER308L can also be used according to Columbus Stainless (2007).

With the drive to reduce manufacturing costs, the focus of this research is to determine the effects of various shielding gases on the mechanical and metallurgical properties of 3CR12 when welded with the more cost effective ER308L welding consumable. The current price of the ER308L and ER309L wires is R189.51 and R296.26 per kilogram respectively. This results in a 36% difference in consumable costs. The ER308L welding wire, although commonly used to weld 3CR12, has previously not been adopted in welding rail wagons, therefore optimised welding using this wire together with the appropriate shielding gas will give an improvement which significantly reduces the cost of producing wagons. The amount of the stainless-steel wire (ER309L) required to build a Jumbo Wagon with dimensions 2592 × 2000 × 14847 mm, for example, is 134.2 kg. The cost difference between the two wires can therefore translate to a total cost of R4.23 million per annum in savings based on a market demand of 300 new wagons being assembled.

Metallurgically, the shielding gas used in a welding process has a significant influence on the overall performance of the weld structure. Aside from protecting the molten metal of the weld pool from atmospheric nitrogen and oxygen, the gas also promotes a stable arc. In gas metal arc welding (GMAW), the gas used has a significant influence on the type of metal transfer during welding. This subsequently affects the efficiency, quality, and overall welding operation (Kah and Martikainen, 2012).

Figure 1-1 illustrates the effects of various gases on the bead contour and penetration of argon, helium and CO_2 shielding gases. The thermal conductivity of argon is low compared to helium which causes a finger-like penetration profile. Helium on the other hand results in a broad but less deep penetration profile due to its high thermal conductivity. Adding reactive shielding gases such as CO_2 and O_2 produces a more desirable effect on the weld pool shown in Figure 1-2 (The Lincoln Electric Company, 2014). The gases are important in several aspects of welding, including arc characteristics and the microstructure of the welded materials. The reaction of oxygen, nitrogen and hydrogen with the weld pool can create a variety of problems, including porosity, excessive spatter, lack of fusion and incomplete penetration (Kah and Martikainen, 2012).

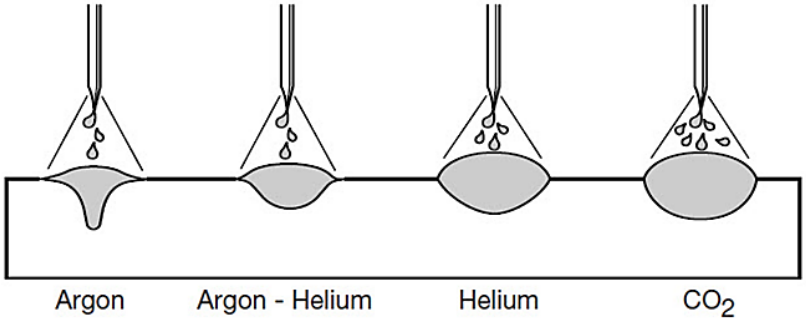

Figure 1-1: Bead contour and penetration patterns for various shielding gases (The Lincoln Electric Company, 2014).

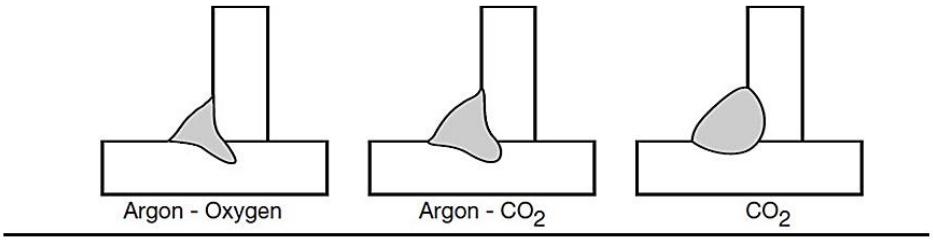

Figure 1-2: Reactive effect of O_2 versus CO_2 additions to argon shielding gas (The Lincoln Electric Company, 2014).

1.2. Problem Statement

Due to lack of available information on utility ferritics such as 3CR12, the International Stainless-Steel Forum (ISSF) published a brochure to fill this knowledge gap and create an awareness of the material, which, due to its low maintenance, high strength and resistance to abrasion is commonly used in the freight industry (International Stainless-Steel Forum, 2018). Process parameters recommended by the manufacturer have been used to qualify welding procedures for production, and although the material has been used to build wagons over the past 36 years, no attempt has been made to optimise the welding process for 3CR12 in order to reduce manufacturing costs in the rail sector.

One such instance wherein such optimisation can be achieved, is to use a cheaper alternative welding wire and suitable gas. Past and present research has, however, shown that there is little information regarding the effect of various shielding gases on the welding of 3CR12 using the ER308L welding wire. Research by Kah and Martikainen (2012), has shown that shielding gas plays a significant role in the metallurgical and mechanical properties of welds and therefore

in order to complete the optimisation of the welding process, further research on the effects of various gas mixtures is required.

1.3. Research Questions

This research aims to answer the following questions:

- What are the effects of pure helium, pure argon, and mixtures of these gases with carbon dioxide and oxygen on the bead contour, penetration, and welding speed when welding 3CR12 with ER308L welding wire?
- Which welding parameters and consequent heat input, provides the best metallurgical and mechanical properties of the weld metal and heat affected zone (HAZ)?
- Which variation in gas mixtures provides the best metallurgical and mechanical properties of the weld metal?

1.4. Hypothesis

Although expensive on its own, it is envisaged that through the subsequent research, the presence of helium in smaller quantities in a gas mixture, will improve welding speed and mechanical and metallurgical properties of 3CR12 wagon welds.

1.5. Aim and objectives

The aim of this research is to determine the effects of various mixtures of Ar, He and CO_2 on the strength, toughness, hardness, corrosion resistance and metallurgical properties of 3CR12 when welded with ER308L wire. The gas mixture that produces superior mechanical and metallurgical properties will be determined through the following objectives:

1. Weld 6 mm 3CR12 plates with ER308L wire using pure Ar and He gas, and various gas mixtures of Ar, He, O_2 and CO_2.
2. Conduct non-destructive tests using visual and magnetic particle inspection to evaluate surface quality of welds.
3. Study microstructural properties of the welds using optical microscope, scanning electron microscope and XRD for phase analyses.
4. Study mechanical properties such as fracture toughness, ductility, and ultimate tensile strength of the samples after welding.
5. Investigate corrosion performance of the welded joints.

1.6. Research Gap

As discussed further in Chapter 2, previous research conducted adds significant value to better understanding the welding of 3CR12, however, it was discovered that there is little information available on the effects of various gas mixtures and ER308L welding wire. With an initiative by rail companies to reduce manufacturing costs and remain competitive, the justification behind the research is to close the gap that exists in the optimisation of the 3CR12 weld process. By investigating the effect of the gases on the microstructure and mechanical properties of ER308L welds, the findings will be implemented in the fabrication of wagons, and in addition will contribute significantly to existing literature and future research on this subject matter.

1.7. Scope of Study

A combination of various gases will be investigated during this research. These gases include pure helium**,** pure argon, and a ternary mixture of 93% Ar, 5% CO_2 and 2% O_2. Other percentage combinations of argon, helium and oxygen will be investigated using a WITT gas mixer. The WITT gas mixer is a 3-part gas mixer manufactured by German based company, WITT-Gasetechnik, a manufacturer of gas related equipment. Due to the high cost of helium, argon will be used as the base gas for the investigation. The gas mixture combinations that will be investigated are discussed in Chapter 3.

1.8. Structure of the Dissertation

Chapter 1 provides the background information of materials that were previously used to build wagons and their disadvantages. It includes the significance of the current research in terms of the aims and objectives as well as the closure of the research gap in achieving the hypothesis.

Chapter 2 summarises the literature review, highlighting the metallurgical properties of 3CR12 and welding of this material in South Africa and around the world.

Chapter 3 provides a detailed description of the investigation, materials, welding parameters, characterisation, etc.

Chapter 4 presents the results and discussion

Chapter 5: Conclusion and recommendations

The dissertation will proceed in the order highlighted in Figure 1.3.

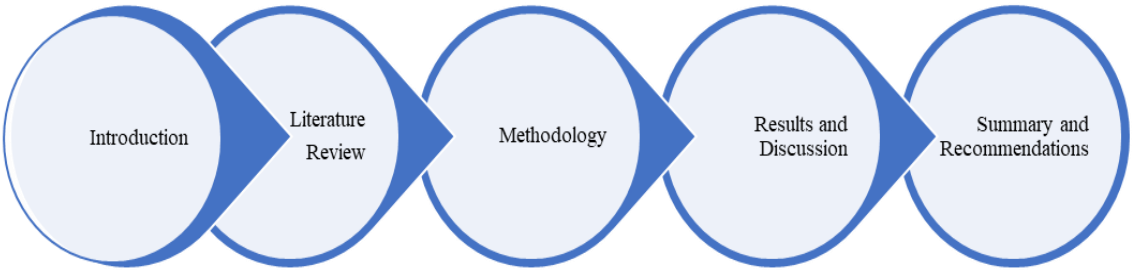

Figure 1-3: Structure of the dissertation.

2.CHAPTER 2

WELDING OF 3CR12 AND AN OVERVIEW OF SHIELDING GASES

2.1. Introduction

Ferritic stainless steel, 3CR12 was developed as a cost-effective alternative to AISI 409 ferritic stainless steel, with good weldability and affordability for mildly corrosive environments. It is an iron-chromium binary alloy containing 10.5-12.5 wt.% chromium as the only major alloying element. The carbon is kept low at 0.025 wt.% and titanium is stabilised to limit chromium carbide precipitation. The chemical composition of the steel is carefully balanced such that some austenite is formed on heating above the critical transformation temperature to limit grain growth (Lakshminarayanan et al., 2011)

Sensitisation may occur when the heat affected zones of welds are cooled through the sensitising temperature range of between 600°C and 700°C. At this temperature, a compositional change may occur at the grain boundaries. If a sensitised material is then exposed to a corrosive environment, intergranular attack may be experienced. In addition, operating and residual stresses can lead to intergranular stress corrosion cracking in these areas. 3CR12 has reasonable resistance to sensitisation after welding. However, sensitisation can occur under specific corrosion conditions and in instances whereby a very low or very high weld heat input has been used, or occasionally with weld overlays depending on exact weld geometry (Columbus Stainless, 2007).

2.2. Overview of 3CR12

Ferritic stainless steels are iron-chromium binary alloys which contain mostly 12 to 30 wt.% chromium as a major alloying element and a maximum of 0.25 wt.% carbon. The name “ferritic” is given to this stainless steel, because the structure is mostly ferritic (BCC α-ferrite) under normal heat treatment conditions (Folkhard, 1988). Some ferritics containing low chromium (10.5 to 12.5 wt.%), are used for general corrosion resistance whilst medium and high chromium grades are used in more aggressive corrosion environments (Lippold and Kotecki, 2005). Chromium is a strong ferrite-forming element which spreads across the α-phase field and suppresses the region where austenite is stable, as shown in Figure 2-1 (Folkhard, 1988).

The 3CR12 alloy differs from most ferritic stainless steels as its chromium content lies within the gamma (γ) loop of the Fe-Cr equilibrium phase diagram (10.5 – 12.5 wt.% Cr) as shown in Figure 2-1. This places the material at the lowest of the stainless-steel family (in terms of corrosion resistance) which enables the grain size to be refined. At room temperature, the microstructure of the as received 3CR12, for the purpose of this research, consists of a fully ferritic structure as shown in the micrograph of the as received material in Figure 2-2.

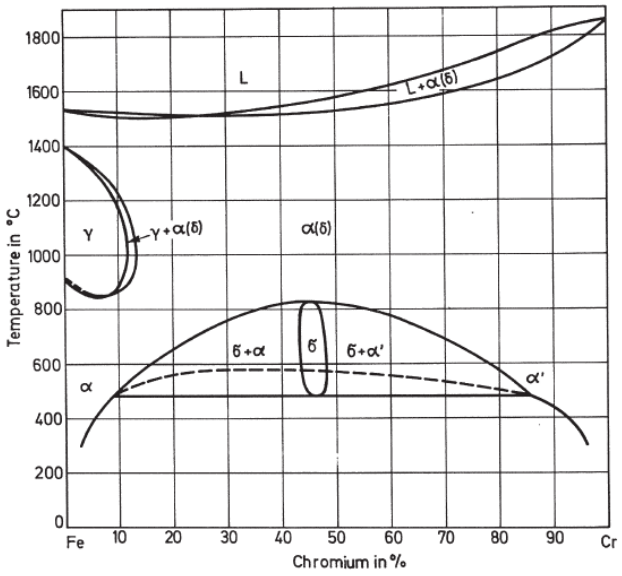

Figure 2-1: The iron-chromium (Fe-Cr) equilibrium phase diagram (Folkhard, 1988).

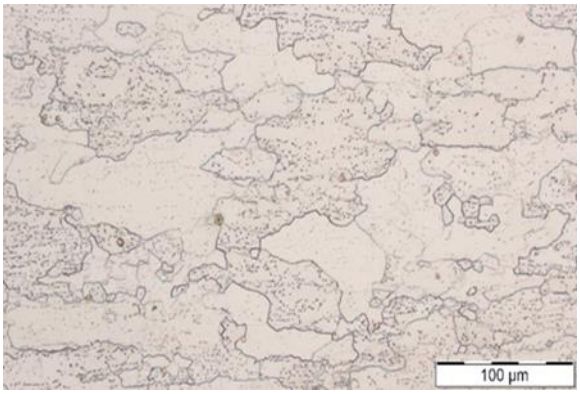

Figure 2-2: Optical micrograph of as received 3CR12 steel.

The chemical composition of 3CR12 is similar to 1.4003 stainless steel, except that 3CR12 contains titanium (Ti) as an additional alloying element. Titanium has a high affinity for carbon. It is used, therefore, like niobium to attract carbon and form stable titanium carbides

(Folkhard, 1988). The chemical compositions of the two steels are listed in Appendix A, Table A-2 (Columbus Stainless, 2007).

The various alloying elements play a role in either promoting ferrite or austenite. Chromium, titanium, silicon, and molybdenum stabilises ferrite, and individually have major effects on the properties of the steel. Chromium improves the general corrosion resistance and resistance to oxidising environments. Silicon improves high temperature oxidation and carburisation resistance. Titanium forms stable carbonitrides to resist sensitisation from welding (Lippold and Kotecki, 2005).

Carbon, nickel, nitrogen, and manganese all promote austenite formation (Lippold and Kotecki, 2005). Like chromium, nickel improves general corrosion resistance but in contrast, it improves the steel's resistance to reducing environments. Whilst carbon decreases the corrosion resistance of the material, it is primarily required for increased strength. Nitrogen also increases the strength of the material and, in addition, improves pitting resistance. Manganese works in contrast to sulphur and phosphorus to that extent that it improves hot cracking resistance and increases the solubility of nitrogen (Lippold and Kotecki, 2005).

The mechanical and physical properties of 3CR12 steel in the hot rolled and annealed condition are shown in Appendix A, Table A-1 (Columbus Stainless, 2007). The thickness of material used in this research is 6 mm.

2.3. Welding of 3CR12 around the world

3CR12 was first invented in South Africa in 1977 by Columbus Stainless Steel and was commercialised in 1981. The aim of creating this new material was to bridge the corrosion resistance requirements gap between high alloyed stainless steels and coated carbon steels. It has been useful in many South African industries including agriculture, mining and power generation, and rail. Of great importance is the use of 3CR12 in coal wagons not only in South Africa but also in countries such as India, United States of America, the United Kingdom, Belgium, and Australia. Prototype wagons placed in service in 1984 are still in operation today with almost no loss in plate thickness (Engineering News, 2012). With extensive use of 3CR12 in the various industries, fabrication of this material with a special focus on welding has become increasingly important amongst scholars.

Research performed in South Africa includes the study of the sensitisation of 3CR12 during welding, a phenomenon that causes intergranular corrosion and ultimately cracking of the

material. Both stabilised and unstabilised 3CR12 was studied by varying the heat inputs and parameters when welding. In the study, welding of un-stabilised 3CR12 using various heat inputs and welding speeds revealed sensitisation of the material at low heat inputs and fast cooling rates. In contrast to this, higher heat inputs provided no sensitisation as the slower cooling rates allowed for martensite formation in the high temperature heat affected zone (HTHAZ) of the weld. The study also concluded that excessive welding speeds, when welding with low heat inputs results in sensitisation (Balsaraf et al., 2013).

In countries like India, 3CR12 is widely used in iron ore wagons. A comparative study of various welding processes on the metallurgical and mechanical properties of 3CR12 was conducted by Lakshminarayanan and Balasubramanian (2012), due to the known of effect of welding on the reduction of toughness, ductility, and corrosion resistance of the material. Friction-stir welding (FSW), gas tungsten arc welding (GTAW), electron beam (EBW) and laser beam welding (LBW) were studied, and it was found that, of the four processes, FSW exhibited the higher weld metal tensile strength because of the fine duplex equiaxed structure of ferrite and martensite. EBW and LBW on the other hand showed higher weld metal toughness in comparison to the other two processes, due to the presence of equiaxed and fine dendritic columnar grains located perpendicular to the crack path (Lakshminarayanan and Balasubramanian, 2012).

Another industry in which 3CR12 is commonly used is sugar processing, whereby low-pressure vessels are fabricated from the dissimilar welding of 3CR12 and S355. In a study by scholars in Thailand, mild steel was welded to 3CR12 with ER308L welding wire using the GTAW process. In this study by Luijan et al. (2020), it was found that the microstructure of the weld contained Widmanstatten austenite, acicular ferrite, and martensite. The presence of martensite together with Cr-rich carbide precipitates formed under certain parameters resulted in better hardness values and tensile strength.

2.4. Welding of 3CR12- General

Ferritic stainless steels do not exhibit good weldability compared to austenitic types (Afrox, 2018). The steels which become fully ferritic at high temperatures tend to form coarse structures which cannot be refined without cold working and recrystallisation (Afrox, 2018). Austenite forms at high temperature in steels with lower chromium content. The austenite can transform to martensite on cooling, which can lead to cracking (Afrox, 2018). Chromium depletion at the grain boundaries also occurs during welding as a result of sensitisation as

depicted in Figure 2-3. This results in weld decay or intergranular corrosion cracking which occurs when the sensitised material is exposed to an applied stress. It is for this reason that ferritic steels, such as 3CR12, with titanium and/or niobium and low carbon and nitrogen have been developed (Kou, 2003).

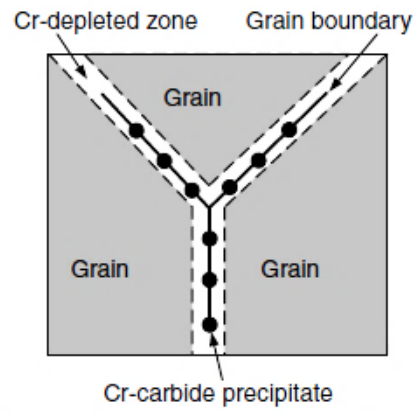

Figure 2-3: Grain boundary microstructure in sensitised stainless steel (Kou, 2003).

A variety of filler metals can be used to weld ferritic stainless steels, depending on the properties and service performance required. Matching or near-matching compositions are used as these will be most compatible with the base metal. Austenitic filler metal is often used to weld second generation stainless steels such as 3CR12 (Lippold and Kotecki, 2005). Austenitic filler metal type ER309L is recommended when welding 3CR12 to mild steel. However, when welding 3CR12 to 3CR12, ER308L or ER316L can be used (Columbus Stainless, 2007).

During cooling, austenite forms at the δ-ferrite grain boundaries in the HAZ, transforming to martensite at lower temperatures. Martensite in ferritic stainless steels has both beneficial and detrimental effects. It causes embrittlement of the structure, and when formed in large quantities, it can cause hydrogen cracking. On the positive side, duplex ferritic-martensitic stainless steels have superior impact toughness properties when compared to fully ferritic and fully martensitic steels of similar compositions (Lippold and Kotecki, 2005).

2.5. Expected heat-affected zone microstructure

Despite the incomplete solid-state phase transformation from ferrite to austenite, upon cooling the high temperature heat affected zone (HTHAZ) normally has a coarse grain size. This is in contrast to the much finer grain size of the low temperature heat-affected zone (LTHAZ) or FGHAZ (fine grained), which is located further away from the fusion line (Du Toit et al., 2010).

To prevent coarse structures and thereby loss of ductility and toughness in the HAZ, a low heat input and a low interpass temperatures are typically advised when welding 3CR12 (Kotecki, 1993). Figure 2-4 shows the typical microstructure of the HTHAZ and LTHAZ in a 1.4003 stainless steel.

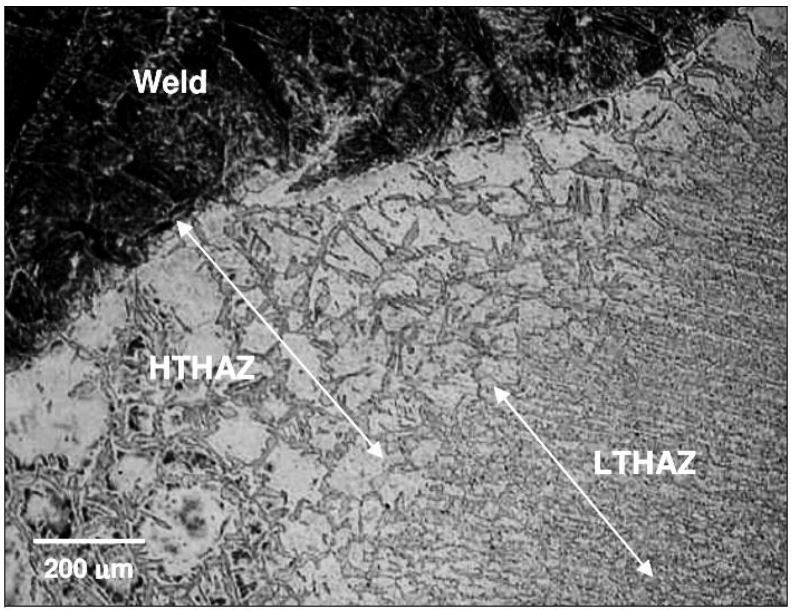

Figure 2-4: The heat affected zone microstructure of 1.4003 stainless steel welded with a heat input of 0.9 kJ/mm (Du Toit et al., 2010)

2.6. Sensitisation

Sensitisation denotes the formation of chromium carbide precipitates that form along the grain boundaries, which leads to a chromium depleted zone near the grain boundaries of materials. The phenomenon results in increased susceptibility to intergranular stress corrosion cracking as chromium is the alloying element responsible for corrosion resistance in stainless steel (Doerr, Kim and Jacobs, 2017). Figure 2-5 shows an example of the various expected microstructures upon examination of etched samples, the first of which is a stepped un-sensitised microstructure (a). In a dual structure (b), there are some “ditches” along the grain boundaries, but no single grain is surrounded by “ditches”. Finally, sensitization is represented by a “ditched” structure where one or more grains in the microstructure are entirely enclosed by “ditches” (c) (Dománková, Kocsisová and Slatkovský, 2014).

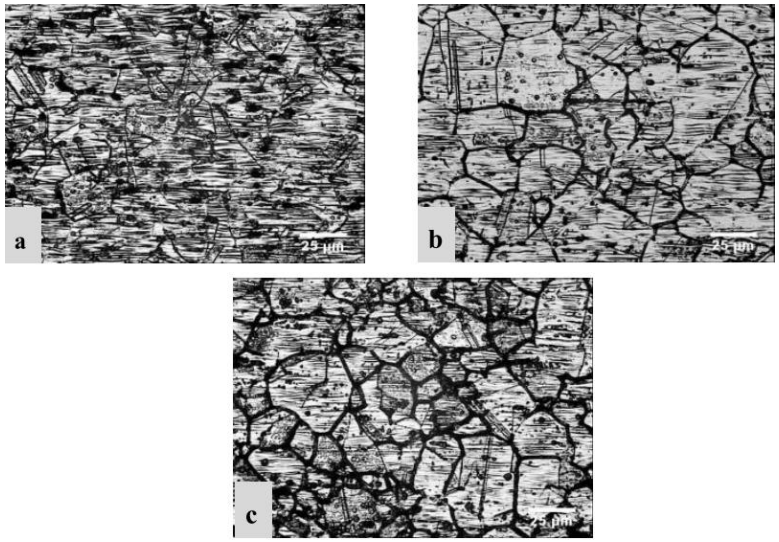

Figure 2-5: Examples of a stepped structure (a), dual structure (b) and ditched or sensitised structure (c) (Dománková et al., 2014).

There are four mechanisms of sensitisation which can occur in ferritic stainless steels. These mechanisms include the chromium depletion theory, strain theory, electrochemical theory, and solute segregation theory. Whilst the first mentioned theory describes the depletion of chromium in the grains adjacent to the precipitated chromium carbide ($M_{23}C_6$) grain boundaries, the strain theory contradicts this phenomenon. According to this theory, extreme plastic deformation at low temperatures (i.e., during cold working), leading to a considerable increase in the dislocation density at the grain boundaries as compared to the matrix, is the leading cause of sensitisation. This imperfect lattice structure enhances the overall diffusion of alloying elements which results in faster sensitisation. In welds, the strain theory is reinforced by the knife-line attack which occurs due to the distorted lattice adjacent to the carbide precipitate at the carbide-austenite or carbide-ferrite interface. The third, electrochemical theory, postulates that a potential difference exists across the metal carbide and the steel matrix. Due to the higher nobility of the metal carbide, accelerated intergranular attack occurs in this region more so in the presence of residual stresses. The last theory, namely solute segregation mechanism, hypothesises that sensitisation occurs in non-sensitised austenitic stainless steel when there is a continuous grain boundary path of a second phase and soluble impure segregates which developed as the result of interactions of solute atoms with vacancies. From the four mechanisms of sensitisation, the only concept that has been proven scientifically is the chromium depletion theory (Amuda and Mridha, 2011).

According to Columbus Stainless (2007), sensitisation of 3CR12 occurs at high temperatures between 600 and 700 ℃, however, it can also occur in certain corrosion conditions and where very low or very high weld heat input is used. This sometimes occurs in weld overlays (weld build up) or multi-pass welds, depending on the joint configuration. The 3CR12 is stabilised with titanium which makes it more resistant to sensitisation, however, a heat input range between 0.5 and 1.5 kJ/mm is recommended by Columbus Stainless (2007), in order to avoid sensitisation and maximise the toughness of the HAZ.

Further studies on the sensitisation behaviour of 3CR12 were conducted in South Africa. One such study entailed gas tungsten arc welding (GTAW) of the material using an austenitic L electrode. It was found that sensitisation occurred when heat input levels were below 0.1 kJ/mm and ferrite-ferrite grain boundaries formed in the HTHAZ. When the heat input was increased above 0.25 kJ/mm, the formation of martensite in the HTHAZ eliminated the continuous ferrite-ferrite grain boundaries and therefore prevented sensitisation in the material (Dahmen et al., 2015).

2.7. Overview of shielding gases

Shielding gases play an important role in protecting the weld pool from atmospheric contamination, in the form of oxygen, nitrogen and water vapour, during welding. The effect of adding various reactive gases (oxygen, hydrogen, nitrogen, and carbon dioxide) to argon and/or helium on the weld metal is discussed.

2.7.1. Carbon Dioxide (CO_2)

Within the high energy of the arc plasma of GMAW welding, the CO_2 molecule separates in a process identified as dissociation (The Lincoln Electric Company, 2014). In this process, free carbon, carbon monoxide, and oxygen are released from the CO_2 molecule at the DC+ anode of the arc. Recombination of the molecules, which generates higher energy levels, takes place at the colder DC- cathode region (the weld pool). This increase in energy levels gives rise to the deep and broad penetration profile of CO_2 welds.

The free oxygen, which does not recombine with the carbon monoxide and carbon, combines chemically with the silicon, manganese, and iron to form silicon, manganese, and iron oxides (The Lincoln Electric Company, 2014). Silicon oxides, otherwise known as silica, form at the surface of the weld pool. With a higher level of carbon dioxide, a greater amount of slag will form. Lower levels of carbon dioxide result in increased amounts of silicon and manganese

retained in the weld. As a result, lower carbon dioxide levels, in a binary or ternary shielding gas blend, increases the yield and ultimate tensile strength of a finished weld.

2.7.2. Oxygen (O_2)

Oxygen reacts with elements in the weld pool to form oxides (The Lincoln Electric Company, 2014). When mixed in small amounts (1%-5%) with argon, it delivers decent arc stability and good weld bead formation. Silicon and manganese combine with oxygen to form oxides thereby compensating for the oxidising effect of oxygen. As with the free oxygen from the carbon dioxide, the silicon oxides float to the surface of the weld bead however, an abundance of slag is formed with CO_2 shielding gas than with mixtures of argon and O_2 shielding gas. shielding.

2.7.3. Hydrogen (H_2)

Hydrogen in small percentages (1-5%) is added to argon for shielding stainless steel and nickel alloys (The Lincoln Electric Company, 2014). Its higher thermal conductivity produces a fluid puddle, which promotes improved toe wetting and permits the use of faster travel speeds.

2.7.4. Binary shielding gas blends

Bipartite shielding gas blends are popular, and they are usually made up of argon and helium, argon and carbon dioxide, or argon and oxygen (The Lincoln Electric Company, 2014). Argon and helium blends are mostly used for welding nickel-based alloys and aluminium. Argon and CO_2 mixtures can be used in pulsed GMAW applications on stainless steel with a maximum CO_2 content of 4%. Argon and oxygen blends accomplish axial spray transfer at lower currents than argon and CO_2 blends. In the past, argon and oxygen mixtures have been linked with high travel speed when welding on thin materials of both stainless and carbon steel.

2.7.5. Ternary Gas Shielding Blends

Three-part shielding gas blends remain a common choice for stainless steel welding (The Lincoln Electric Company, 2014). Helium delivers superior thermal conductivity for short-circuiting transfer applications in stainless steel base materials. Additions of 55% to 90% are combined with argon and 2.5% CO_2 for short-circuiting transfer. This three-part mixture is preferential in decreasing spatter, improving weld pool fluidity, and for creating a flat weld bead appearance. Tri-mixes are available either as argon-rich (~80% Ar) and helium-rich (~90% He). Helium-rich gases are used for short-circuit transfer and include a small amount of argon for arc stabilisation and a very small amount of CO_2 for penetration and cleaning. Argon-rich mixes consist of 1 - 2% CO_2 with the remainder made up of helium. Argon-rich

mixes are generally used for spray transfer, which occurs because of the high argon content. Argon permits the use of spray transfer at low voltages whilst helium provides excellent wetting and flat bead profiles (Schweighardt, 2007).

Shielding gas selection affects the quality and productivity of welded components. The correct gas for a given arc welding process can improve speed, quality, and deposition rate (Schweighardt, 2007). In pure form, argon, helium, and carbon dioxide can be used individually in arc welding processes whilst oxygen, nitrogen and hydrogen are used in gas mixtures. Depending on the process and material, many different gas mixtures can be used.

2.8. Effect of shielding gas on the welding of stainless steel

When using GMAW, the influence of the various shielding gases upon the chemical composition of the weld metal must also be considered. Argon, helium, and a combination of these mixtures are used for welding stainless steel (ESAB, 2011). Due to the lower thermal conductivity of Ar, the arc energy is less uniformly dispersed, resulting in a more concentrated high energy core. This produces a stable arc with a deep penetration pattern. However, with pure helium, a broad and shallow penetration is achieved (Kou, 2003).

Argon gas with lower levels of oxygen or carbon dioxide is frequently used in the welding of stainless steels. Various gas characteristics are shown in Appendix A, Table A-3 (Kah and Martikainen, 2012). A study titled 'Shielding gas influence on the ferritic stainless-steel weldability' showed that shielding gas compositions had a significant impact on the chemical composition and microstructure of a weld deposit. The study confirmed that when welding ferritic stainless steel with austenitic wire, an increase in CO_2 within the shielding gas increased the carbon content in the weld metal, resulting in martensite formation. Depending on the amount of titanium or niobium, losses of alloying elements occurred owing to the presence of either O_2 or CO_2 (Kah and Martikainen, 2012).

A study conducted for the welding of AISI 304L austenitic stainless steel that was welded with the GMAW process with ER308L welding wire showed the effect of using various shielding gases on the mechanical properties and microstructure of weldments. The research reveals higher tensile strength and hardness values in the weld compared to the base metal when there is an increase in the amount of CO_2 in a shielding gas. High levels of CO_2 in shielding gas mixtures also influences the toughness of the weld to such an extent that it decreases the amount

of delta ferrite content in the weld metal which results in a decrease in the toughness (Anand et al., 2013).

As a result of the short supply and rising costs of argon gas, the effects of alternative root shielding gases in the weld microstructure of 304L stainless steel welded with GTAW were investigated. Pure argon, pure nitrogen, and nitrogen with 10% helium were used in the investigation. It was found that the nitrogen rich gas increased the nitrogen content of the weld, which resulted in a decrease in ferrite content. However, there was no indication of hot cracking (Panmongkol and Phung-on, 2021).

The effects of consumables on the properties of 1.4003 stainless steel joined by GMAW were evaluated. The differences in weldability and mechanical properties when using ER309LSi, ER308LSi, and ER316LSi austenitic stainless-steel consumables were assessed. The ER309L and ER316L welding wires had better corrosion resistance and impact toughness properties than ER308L welding wire (Taban et al., 2012). Further research was performed on the sensitisation behaviour of welded 1.4003 stainless steel. Various welding parameters were used to determine the effects of high and low heat inputs on the HTHAZ of the weld. It was found that excessive welding speeds promoted sensitisation during low heat input welding (Balsaraf *et al.*, 2013).

2.9. Effects of shielding gas on metal transfer

Various welding processes such as Gas metal arc welding (GMAW), Gas tungsten arc welding (GTAW) or Shielded metal arc welding (SMAW) can be used to join 3CR12 material.

GMAW is an arc welding process which joins metals by creating an arc that is formed between a filler metal electrode and base metal. The heat forms a molten weld pool which is protected by an externally supplied shielding gas (The Lincoln Electric Company, 2014).

There are three forms of metal transfer that can be used in the GMAW process i.e., short arc (dip transfer), spray arc and pulsed welding as shown in Figure 2-6: Illustration of metal transfer from left to right, (a) short arc, (b) spray arc and (c) pulsed welding (Kapustka, 2012). The type of arc used is dependent on the thickness of material, joint type, and position of welding (ESAB, 2011).

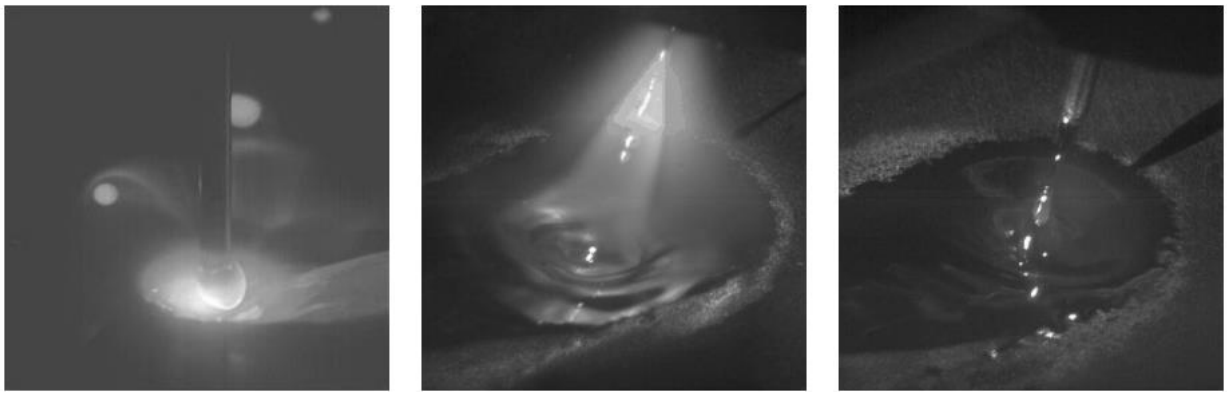

(a) (b) (c)

Figure 2-6: Illustration of metal transfer from left to right, (a) short arc, (b) spray arc and (c) pulsed welding (Kapustka, 2012).

Short arc welds are created from low voltages and currents, and are mainly used for root runs, joining thin material and for certain positions of welding. Spray arc is achieved at higher currents and voltages and is most suitable for down hand welding and thicker materials. The current and voltage for pulsed arc welding is less than that used for spray arc transfer. A voltage pulse onto the base metal creates an artificial spray arc with one drop of metal per pulse in the short arc range. This mode of transfer is used when welding stainless steels, for all positions of welding and when low heat input is required (ESAB, 2011).

Shielding gases and the contact tip to work distance interact to a larger or smaller degree on the electrode wire and weld bead, depending on the metal transfer mode, and this in turn affects the quality of the weld bead (Taylor et al., 2010). It was found that shielding gases with low ionisation potential and high oxidation potential improves arc stability (S. Azar and Diplas, 2022). Argon for example has a low ionisation potential and low oxidation potential as well as low heat conductivity. This allows for opening of the arc and stability at low currents as well as spray transfer (Taylor et al., 2010). Both argon and helium are inert gases, however, helium has a higher ionisation potential and therefore requires a much higher arc voltage, thereby producing a higher arc power density. Although helium is a good thermal conductor, the higher arc voltage implies a lower arc stability when compared to argon. Whilst not studied in adequate detail, it is anticipated that adding helium to argon will alter the structure and characteristics of the plasma arc which in turn affects the metal transfer and weld quality (Rao, Hu, and Liao, 2009).

In a study by Rhee and Kannatey-Asibu (1992), on the "Observation of Metal Transfer during Gas Metal Arc Welding", it was found that adding more CO_2 to argon increases the transition current from globular to spray. It was also found that with pure CO_2 and helium shielding gas, the drop frequency increased slowly with increasing current. Shielding gas mixture with high argon content above 85% allows for high productivity and a spray transfer mode. Aside from the conventional O_2 and CO_2 blends, adding helium to argon can increase the weld metal deposition rate by up to 15%. A pulsed spray transfer on the other hand, can be achieved with reduced splatter when welding plain carbon steels with an argon content of 95% (Garth and Lyttle, 2007).

The type of metal transfer during GMAW, has a large effect on the weld pool characteristics, and this essentially influences weld penetration, solidification, heat flow and the range of welding positions and parameters (Zhao et al., 2019). According to Mathison (2008), globular metal transfer, a high heat input process, is generally used to weld in the flat and horizontal position, due to large droplet size and difficulty in controlling the weld pool in the vertical and overhead position. The effects of metal transfer modes on the mechanical properties of 10mm thick welded 3CR12 was, however, studied in 2019 and for the gas metal arc welding (GMAW) method, the study found that globular down hand welding revealed higher mechanical properties than spray down hand. Furthermore, it was found that when welding vertically globular metal transfer showed higher mechanical properties when welding vertical up as compared to vertical down (Madyira et al., 2019).

In most cases, the short circuit transfer method is used to weld out of position welds with a 75 percent argon/ 25 percent CO_2 shielding gas. Due to the low energy and heat input, this method is used to weld thin gauge materials and for root runs in pipes or plates with no backing material. In contrast, the spray transfer method, which is a high heat input process, is used to weld thicker materials generally in flat or horizontal positions due to the deep finger-like penetration produced (Mathison, 2008).

2.10. Effects of shielding gas on weld productivity

It has been previously discussed that choosing an appropriate shielding gas and using an optimised flow rate will result in increased productivity, lower gas consumption and improved microstructural and mechanical properties. For example, in a study by Mvola and Kah (2016), it was observed that helium gas improves travel speed which in turn increases productivity. It

was also found that the addition of CO_2 results in wider and deeper weld penetration which can allow for increased travel speeds.

The flow of the shielding gas also affects the welding speed in terms of the heat transfer efficiency. By reducing the shielding gas flow rate, welding speed can increase as the heat transfer also increases. In a study by Campbell et al., (2012), an argon/oxygen (80/20) mix was used to weld DH36 grade steel, a low carbon steel used in ship building. It was found that in environments where there is little to no draft, gas flow rates down to 6L/min can be used whilst producing sound quality welds. The lower flow rate showed an increase in penetration of the weld along with distortion and higher temperatures, implying that faster travelling speeds can be used.

3.CHAPTER 3

MATERIALS AND METHODS

This chapter details the experimental plan that was developed throughout this investigation to evaluate the effects of various gas mixtures on the mechanical and metallurgical properties of 3CR12 welds using the ER308L welding wire.

3.1. Materials and Consumables

3.1.1. Parent material

The 3CR12 material used in the experimental procedure was received in a hot rolled and annealed (between 780 and 800 °C) condition. The 6 mm ×1250 mm × 2500 mm sheets were supplied by Columbus Stainless (Pty) Ltd and consisted of the chemical composition and mechanical properties as per the material data sheet shown in Table 3-1 and Table 3-2.

Table 3-1: Chemical composition of 3CR12.

	%C	*%Si*	*%Mn*	*%P*	*%S*	*%Cr*	*%Ni*	*%Ti*
Min	-	-	-	-	-	10.50		4(C+N)
Max	0.030	1.00	2.00	0.040	0.030	12.50	1.50	0.6
Actual	0.012	0.83	0.73	0.025	0.001	11.2	0.63	0.14

Table 3-2: Mechanical properties of 3CR12.

	R_p0.2 (MPa)	*R_m (MPa)*	*Elongation (%)*	*Brinell Hardness*
Min	300	460	20	-
Max	450	-	-	220
Actual	447	558	24	183

The Kaltenhauser ferrite factor (KFF) that is used to quantify the ratio of ferrite- to austenite-forming elements is calculated using Equation 3- 1. A high factor value indicates more ferrite stability which implies that, upon cooling less austenite forms in the microstructure of a weld. This results in reduced martensite content (Khosla *et al.*, 2018). For the as received 3CR12 material, the KFF factor is calculated to be 12.84.

$$KFF = Cr + 6Si + 8Ti + 4Mo + 2Al - 40(C + N) - 2Mn - 4Ni \quad \text{Equation 3-1}$$

3.1.2. Welding wire

The ER308L welding wire, designated as EN ISO 12072-G 19 9 L (British Standards Institution, 2017) was used in this experiment. The chemical composition of austenitic steel wire according to BS EN 14343 is listed in Table 3-3, along with the composition of the wire used as per the material data sheet.

Table 3-3: Chemical composition in wt.%.

	%C	%Si	%Mn	%P	%S	%Cr	%Ni	%Mo	%Cu	%Co
Min	-	-	1.00	-	-	19.00	9.00	-		-
Max	0.030	0.65	2.50	0.03	0.02	21.00	11.00	0.5	0.50	-
Actual	0.012	0.34	1.87	0.015	0.011	19.65	9.55	0.03	0.08	0.021

3.1.3. Shielding Gases

A combination of various gases was investigated during this research. These included pure helium, pure argon, and a ternary mixture of 93% Ar, 5% CO_2 and 2% O_2. Other combinations were investigated using a WITT gas mixer. Due to the high cost of helium, argon was used at the base gas for these mixtures. The gas mixtures combinations that were investigated are shown in Table 3-4.

Table 3-4: Gas mixtures used in this experiment.

	%Ar	*%He*	*%CO_2*	*%O_2*	*Description*
1	-	99.99	-		Pure
2	95	-	5	-	Mix
3	98	-	2	-	Mix
4	73	25	2		Mix
5	75	25	-	-	Mix
6	98	-	0	2	Mix
7	50	50	-	-	Mix
8	93	-	5	2	Coogar 93

3.2. Methodology

The overall methodology is summarised in Figure 3-1. After passing non-destructive testing (magnetic particle and visual inspection), the welded plates were marked, cut, and machined for the various mechanical and metallurgical tests. Welds were assessed for intergranular corrosion using Practice W and Practice Z of ASTM 763-93 (ASTM International, 2004), as well as a potentiostatic etch which followed the oxalic acid etch test.

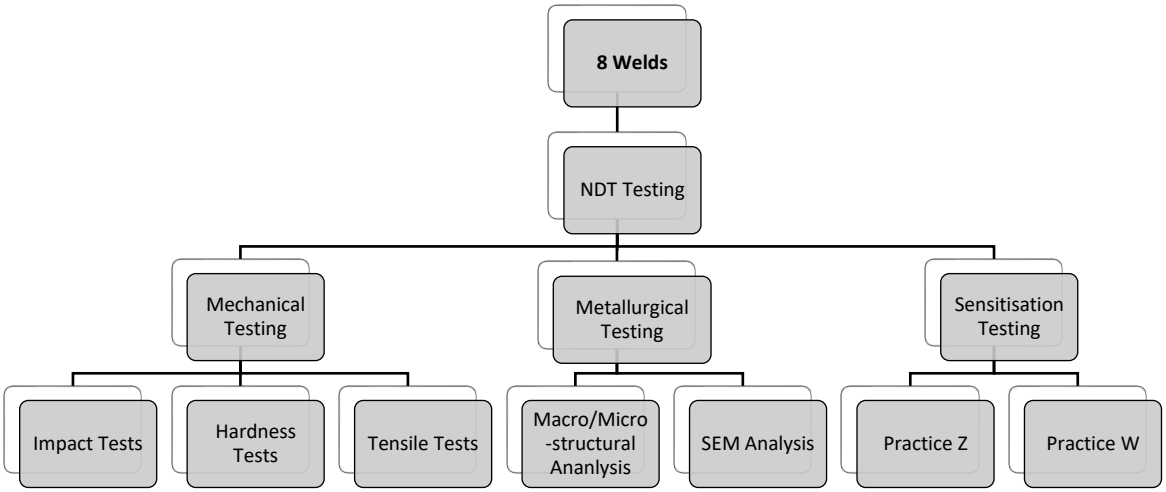

Figure 3-1: Experimental plan developed for investigation.

3.2.1. Welding

Test plates with a size of 150 mm × 400 mm × 6 mm (shown in Figure 3-2) were cut and prepared with a 30° bevel and 1.5 mm landing. The root gap and plate preparation are shown in Figure 3-3.

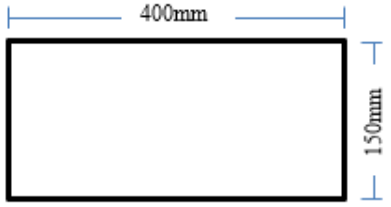

Figure 3-2: Plate dimensions 150 mm × 350 mm

Figure

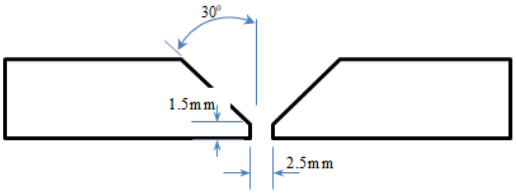

Figure 3-3: Sketch of joint design and edge preparation.

Gas metal arc welding was used for welding the samples. The welding parameter range was chosen based on the wire size (1 mm) and manufacturers' recommendations. The recommended voltage settings for 1 mm ER308L welding wire are between 15 V and 28 V with a current between 80 A and 240 A. These parameters were the basis used to weld the test plates using a gas flow rate range between 15 l/min and 20 l/min. The welds of plates 1 to 4

are shown in Figure 3-5 for illustrative purposes. The wire feed speed and welding speed was also recorded for the calculation of the heat input. The plates were welded using the welding parameters and heat inputs shown in Table 3-5. The range of heat inputs varied from 0.4 kJ/mm to 0.9 kJ/mm, and this fell within the ranges recommended by Columbus Stainless Steel. To maintain consistency and reduce human and machine errors, the same welder and welding equipment were used.

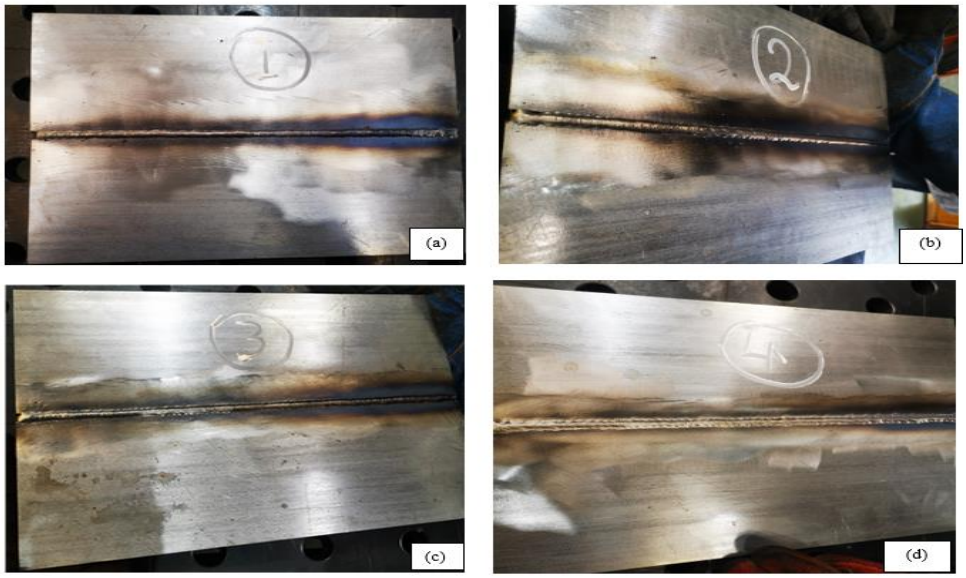

Figure 3-4: As welded plate for gas mixtures: (a) He, (b) 95Ar-5CO_2; (c) 98Ar-2CO_2; (d) 73Ar-25He-2CO_2.

Table 3-5: Calculated welding parameters used in the investigation.

Gas	*Test No.*	*Voltage* *V*	*Current* *A*	*Gas flow rate l/min*	*Wire feed speed mm/min*	*Time taken to weld S*	*Welding speed cm/min*	*Heat Input kJ/mm*
He	1	28.2	121	20	7014	48	25.0	0.7
		28.4	118	20	7014	48	25.0	0.6
95%Ar, 5%CO_2	2	21	110	18	5320	113	21.2	0.5
		22	150	18	8884	93	25.8	0.6
98% Ar, 2% CO_2	3	21	110	18	5500	107	22.4	0.5
		22	150	18	8748	101	23.8	0.7
73 Ar, 25He, 2CO_2	4	21	105	18	5308	117	20.5	0.5
		22	137	18	8080	90	26.7	0.5
75 Ar, 25He	5	21	100	18	4552	97	24.7	0.4
		22	140	18	8516	77	31.2	0.5
98Ar, 2O_2	6	21	117	18	5096	123	19.5	0.6
		22	151	18	8184	134	17.9	0.9
50Ar, 50He	7	21	100	18	5408	93	25.8	0.4
		22	100	18	5408	102	23.5	0.4
93Ar, 2O_2, 5CO_2	8	22.05	114.5	15	10762	112.24	21.4	0.6
		22.05	114.5	15	10762	112.24	21.4	0.6

3.2.2. NDT testing

Once the plates were welded, the welds were examined using non-destructive testing in the form of Visual Testing (VT) and Magnetic Particle Testing (MT). VT was performed to check for weld discontinuities that are visible. If no discontinuities were seen, then MT was performed. MT is a non-destructive technique that is used to identify surface or subsurface defects in the welds. Prior to MT, the plates were inspected once again. The test area and at least 3cm on either side of the weld must be free from slag, spatter, oil, or any other form of dirt that can inhibit testing or mask discontinuities. Aside from slight spatter, which was buffed away where necessary, the plates were in an acceptable condition for testing. The MT process entailed magnetising the weld area, using a handheld yoke as shown in Figure 3-5. The weld area was sprayed with white contrast paint and thereafter ferromagnetic particles were sprayed. The fine iron particles are attracted to the magnetic flux leakage fields and cluster to form an indication over a discontinuity if present.

Figure 3-5: Photograph of magnetic particle testing of welded plate

3.2.3. Mechanical testing

3.2.3.1.Hardness testing

Micro-hardness testing was carried out on the samples. The Vickers micro-hardness tester was used to evaluate the hardness change across the weld, the HAZ and parent metal according to

BS EN ISO 9015-1(British Standards Institution, 2011). A hardness profile, which is discussed in the succeeding chapter, was drawn up and measurements taken 1 mm apart from each other from the parent metal, through the HAZ and through the weld. A load of 0.5 kgf (kilogram-force) was used with a dwell time of 10 seconds.

3.2.3.2.Charpy testing

Impact testing was performed at room temperature (23 °C), -20 °C and -7 °C respectively. After removing samples from the freezer and, before testing, the temperatures were measured using an infrared thermometer to confirm temperature values. The testing was performed according to DIN EN ISO 148-1 (European Committee for Standardisation, 2011). The impact testing was performed on the weld metal zone as per the sketch in Figure 3-6. An example of the machined test pieces is shown in Figure 3-7.

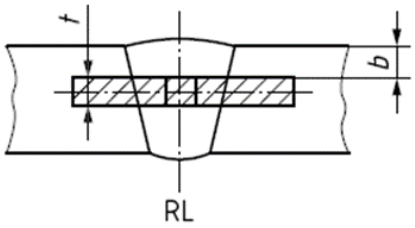

Figure 3-6: Dimensions of the impact test specimen (European Committee for Standardisation, 2013).

b = 1 mm

RL = Reference line at centre of weld

t = 4 mm

Figure 3-7: Sample of machined Charpy Impact test pieces.

3.2.3.3.Tensile testing

Tensile testing was performed at room temperature according to EN ISO 6892-1. Figure 3-8 shows the dimensions of the tensile specimens which are extracted from ASTM E8-13a (ASTM International, 2013). An example of the machined tensile samples is shown in Figure 3-9.

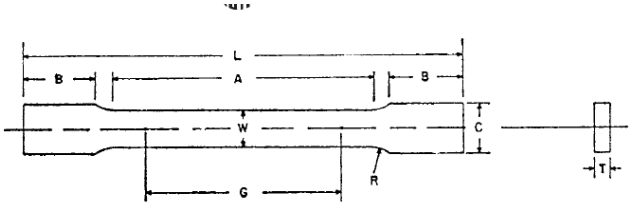

	Dimensions		
	Standard Specimens		Subsize Specimen
	Plate-Type, 40 mm [1.500 in.] Wide	Sheet-Type, 12.5 mm [0.500 in.] Wide	6 mm [0.250 in.] Wide
	mm [in.]	mm [in.]	mm [in.]
G—Gauge length (Note 1 and Note 2)	200.0 ± 0.2 [8.00 ± 0.01]	50.0 ± 0.1 [2.000 ± 0.005]	25.0 ± 0.1 [1.000 ± 0.003]
W—Width (Note 3 and Note 4)	40.0 ± 2.0 [1.500 ± 0.125, -0.250]	12.5 ± 0.2 [0.500 ± 0.010]	6.0 ± 0.1 [0.250 ± 0.005]
T—Thickness (Note 5)		thickness of material	
R—Radius of fillet, min (Note 6)	25 [1]	12.5 [0.500]	6 [0.250]
L—Overall length, min (Note 2, Note 7, and Note 8)	450 [18]	200 [8]	100 [4]
A—Length of reduced section, min	225 [9]	57 [2.25]	32 [1.25]
B—Length of grip section, min (Note 9)	75 [3]	50 [2]	30 [1.25]
C—Width of grip section, approximate (Note 4 and Note 9)	50 [2]	20 [0.750]	10 [0.375]

Figure 3-8: Dimension for tensile test pieces (ASTM International, 2013).

Figure 3-9: Sample of machined tensile test pieces.

3.2.4. Metallurgical testing

Macroscopic analysis of the weld area was completed using a stereo microscope while microanalysis was completed using an optical microscope. The specimens were prepared as follows:

3.2.4.1.Macroscopic Examination

The welded test specimens were cut, ground, polished and etched in accordance with ISO 17639 on one side in order to clearly reveal the fusion line, the HAZ and the build-up of the runs for the macro examination. The weld geometry, number and size of passes and depth of penetration were evaluated on the Olympus SZX16 Stereo Scope and a comparison of the extent of the HAZ (heat affected zone) between the various samples was also carried out as

well as an analysis for surface imperfections such as cracks, undercuts, excessive throats, and convexity. Internal imperfections such as cracks, porosity, metallic inclusions, lack of fusion, lack of penetration, and slag were noted and discussed along with joint geometry imperfections such as root gap, root face, angle of chamfer and misalignment.

3.2.4.2.Microscopic Examination

Using the Struers Discotem-100 cutting machine and an abrasive cut-off wheel for medium soft ferrous metal (100 < HV < 500), the samples for microscopy were cut and then mounted, ground, polished and etched to reveal the fusion line, HAZ and parent material. To avoid overheating when cutting the samples, the machine is equipped with a cooling system that uses a Struers brand coolant additive solution. The samples were then mounted with Multifast resin and ground using 220, 1000 and 1200 grit papers respectively. Water was used as a lubricant for all the grinding steps. Polishing was then performed using the 9 µm, 3 µm, 1 µm suspensions and colloidal cloth with the corresponding suspensions. Two different etchants, namely, Villella's reagent and Aqua-regia were then used to etch the samples. Villella's reagent was mixed using 1 g of picric acid, 5 ml of hydrochloric acid and 100 ml of ethanol. This reagent was used to reveal the microstructure of the heat affected zone. Aqua regia revealed the microstructure of the weld and was mixed using nitric acid and hydrochloric acid at a 1:3 ratio.

The microstructures were captured on the Olympus GX71 Optical Microscope at a magnification of 10×, and the areas of focus were the HAZ and the weld. Voids (porosities, shrinkage, cavities, micro-cracks), special phases such as sigma-phase in stainless steel, grain size and segregation in the weld structure, HAZ and the base metal structure were examined.

3.2.4.3.Scanning electron microscope (SEM)

The Zeiss Merlin VP Compact is a field-emitter scanning electron microscope (SEM). The SEM with Energy Dispersive X-Ray Spectroscopy (EDS) was used to examine the different zones and determine the approximate composition of the weld metal. This also assisted in determining whether the material has been sensitised or not.

3.2.4.4.X-ray Diffraction Analysis (XRD)

The Panalytical Empyrean XRD model that is equipped with a Cu kα X-ray source was used to determine the various phases (ferrite, austenite, and martensite) present in the weld metal and HAZ. The source was accelerated at a voltage of 45 kV, current of 40 mA and scanning

from 20˚ to 120˚ angles at a step size of 0.02. After obtaining diffractographs, identification of the phases was performed using the Highscore software with the Rietveld method.

3.2.5. Sensitisation testing

Sensitisation in the heat affected zone of a ferritic stainless-steel weld occurs because of various factors. These include welds in incorrectly annealed material, overlapping in the heat affected zone of multiple pass welds, continuous cooling after welding at low heat input or welding at excessive high heat inputs. The amount of carbide precipitation and chromium depletion can be detected by means of a bend test after submerging the samples in a boiling acid test solution, or through microscopic evaluation after electrolytic etching. These tests are discussed in further detail in this chapter.

3.2.5.1.ASTM A 763-93

The ASTM A 763-93 (ASTM International, 2004) standard was used for detecting the susceptibility to intergranular attack in the welded samples. Practice Z was chosen as the most acceptable method when performing sensitisation tests on 3CR12. This practice tests embrittlement due to sensitisation by submerging the weld samples in boiling sulphuric acid. Practice W was also used to detect the presence of chromium carbides.

3.2.5.2.Practice W

Practice W was modified by using Vilella's reagent instead of oxalic acid in electro-etching the microstructure samples. Villella's reagent was mixed using 1g of picric acid, 5ml of hydrochloric acid and 100 ml of ethanol. This reagent was used to reveal the microstructure of the heat affected zone and weld and the etching was done by pouring the reagent on each sample until the heat affected zone and weld started changing colour. To electro-etch, a direct current power supply was used with a voltage of 63 V, current of 3.17 A and the samples were immersed, with a stainless-steel cathode touching a small portion of the sample, for 1 minute. The microstructure images were then taken at a magnification of 10 X and the areas of focus were on the low-temperature heat affected zone LTHAZ, HTHAZ and the weld.

3.2.5.3.Practice Z

Practice Z requires the immersion of samples in a boiling copper-copper sulphate- 16% sulphuric acid solution to test the susceptibility of ferritic stainless steel to intergranular corrosion. The solution contains approximately 6 wt. % of anhydrous copper sulphate, and 16

wt. % of sulphuric acid. SEM was used to analyse the materials microstructure. Bend test evaluation exposes the risk that the heat affected zone will not be completely strained and reveals fissures which could also be the result of poor ductility in the weld**.** The original experimental plan was modified during the investigation. Samples that underwent the original boiling acid test, suffered aggressive attack in the heat affected zone which hindered evaluation of the microstructures. After further research, it was found the experiment required modification. The standard sensitisation test is too aggressive for 11%-12% chromium stainless steels and a modification was necessary in order to attack the regions of the sample that contain less than 12% chromium (Hu et al., 2020). More samples were cut and prepared from the original weld plate and tested according to a modified acidic solution. The acid concentration was reduced from 16 vol.% to 6 vol.% and the boiling time from 24 hours to 15 hours. A 1000ml Erlenmeyer flask was used with copper shavings to cover each sample that was submerged in the test solution. An Allihn condenser was also used to maintain the volume of the solution during the test. The experimental set-up with solution is shown in Figure 3-10.

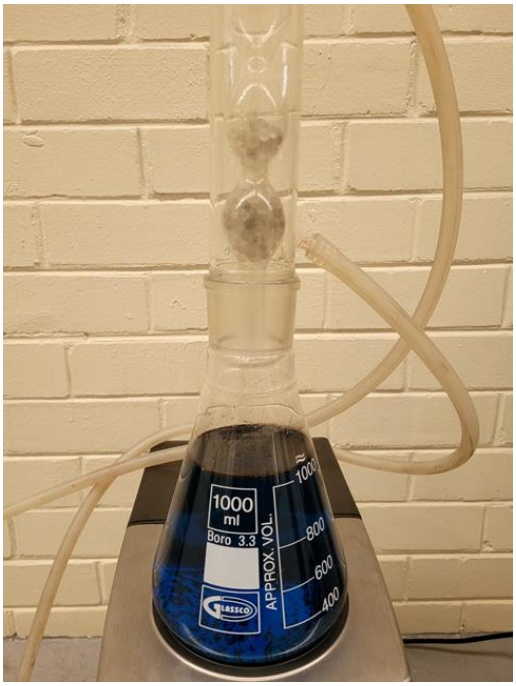

Figure 3-10: Practice Z experimental set-up.

4.CHAPTER 4

RESULTS AND DISCUSSION

4.1. Welding

4.1.1 Comparison of output parameters

A comparison of the welding speed and heat input between samples was analysed to understand the effects of these parameters on productivity and metallurgical properties of the weld and the heat affected zone. The welding speed was measured during the weld test by timing the start to end of the weld whilst the test piece was welded. The length of the plate was then divided by the time to determine the speed. Values of the average heat input and travel speeds are shown in Table 4-1.

Table 4-1: Average values for heat input and welding speeds.

Gas	*Test No.*	*Travel speed cm/min*	*Heat Input kJ/mm*
He	1	25.0	0.65
95%Ar, 5%CO_2	2	23.5	0.55
98% Ar, 2% CO_2	3	23.1	0.60
73 Ar, 25He, 2CO_2	4	23.6	0.50
75 Ar, 25He	5	28.0	0.45
98Ar, 2O_2	6	18.7	0.75
50Ar, 50He	7	26.2	0.40
93Ar, 2O_2, 5CO_2	8	21.4	0.60

The heat source for GMAW is an electric arc. The power density of the heat source depends on the type of welding process. As the power density of the heat source increases, the heat input required to weld a workpiece decreases. The heat source efficiency η for gas metal arc welding is demonstrated in Figure 4-1 as an average of 0.85 (Kou, 2003).

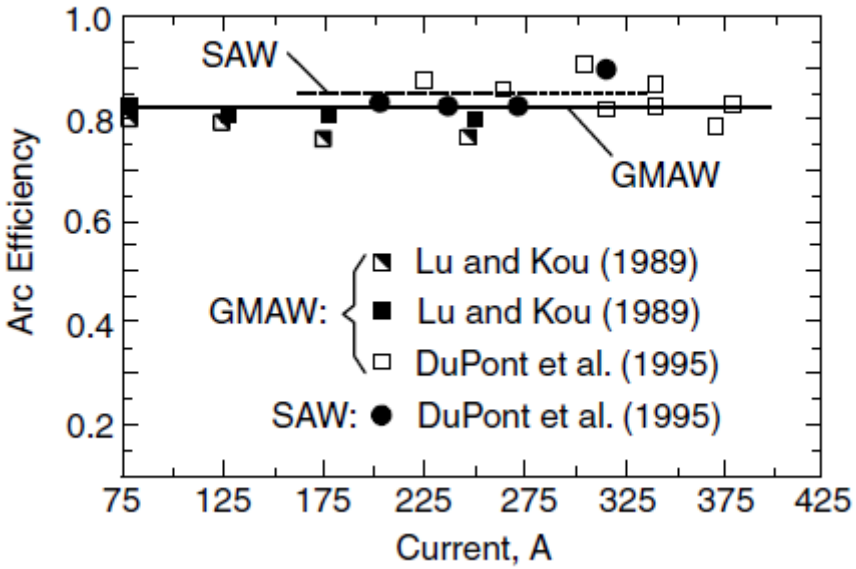

Figure 4-1: Arc efficiencies in GMAW and SAW (Kou, 2003).

This efficiency factor considers losses of the arc power through radiation, convection, and conduction to the surrounding atmosphere, un-melted electrode, contact tip and gas nozzle. The arc efficiency is used to calculate the weld heat input as shown in Equation 4-1 (Quintino, Liskevich and Vilarinho, 2013). The equation shows that heat input is directly proportional to the current and voltage and indirectly proportional to the welding travel speed.

$$H = \frac{U\ x\ I}{TSweld}\eta \qquad \text{Equation 4-1}$$

Where;

H – Heat input

U – Welding voltage

I – Welding current

TS_{weld} – Welding travel speed

η – heat source efficiency

Figure 4-2 and Figure 4-3 show comparison charts for the average welding speed and heat input respectively. Sample 5 (75%Ar, 25%He) displayed the fastest travel speed and correspondingly one of the lowest heat inputs at 0.4 kJ/mm. Conversely, Sample 6 (98%Ar, 2%O_2) has the slowest travel speed and highest average heat input. With comparison of the results, it can be

seen that all samples with helium content proved to have faster travel speed. These findings are in accordance with the observation reported by Mvola and Kah (2016). Similarly, an increase in the addition of CO_2 to argon showed faster travel speeds at the same gas flow rates. It was also observed that the binary mixture of Ar and CO_2 (Sample 3) allowed for faster travel speed when compared to Ar and O_2 (Sample 6). The low travel speed of 18 cm/min and a high heat input of 0.7 kJ/mm for the Ar/O_2 mix can be attributed to the low oxidation potential and heat conductivity of argon (Taylor et al., 2010).

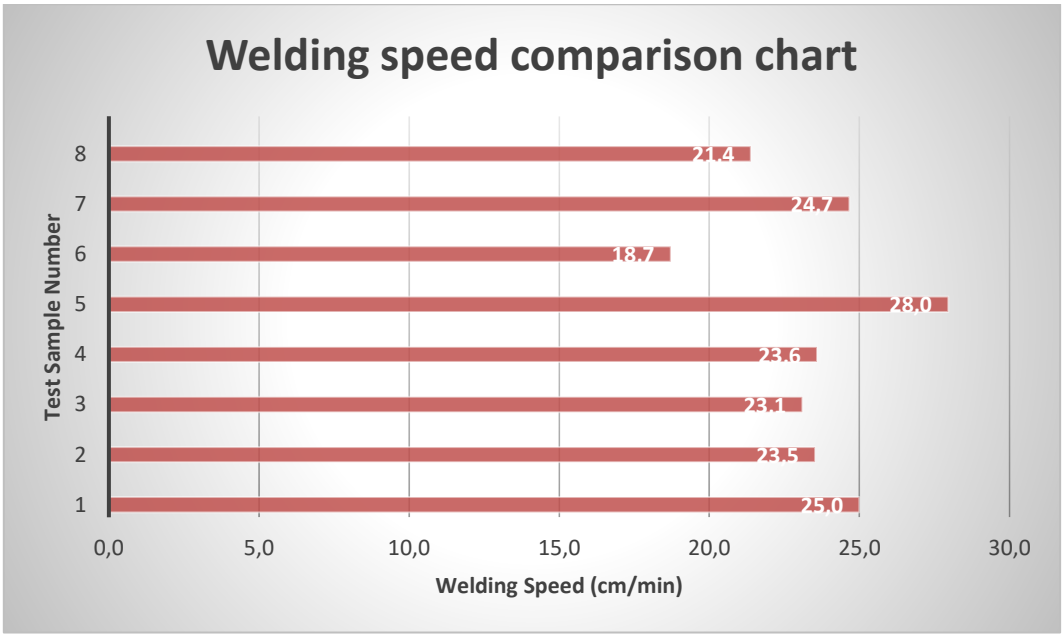

Figure 4-2: Comparison chart depicting difference in average welding speeds per sample.

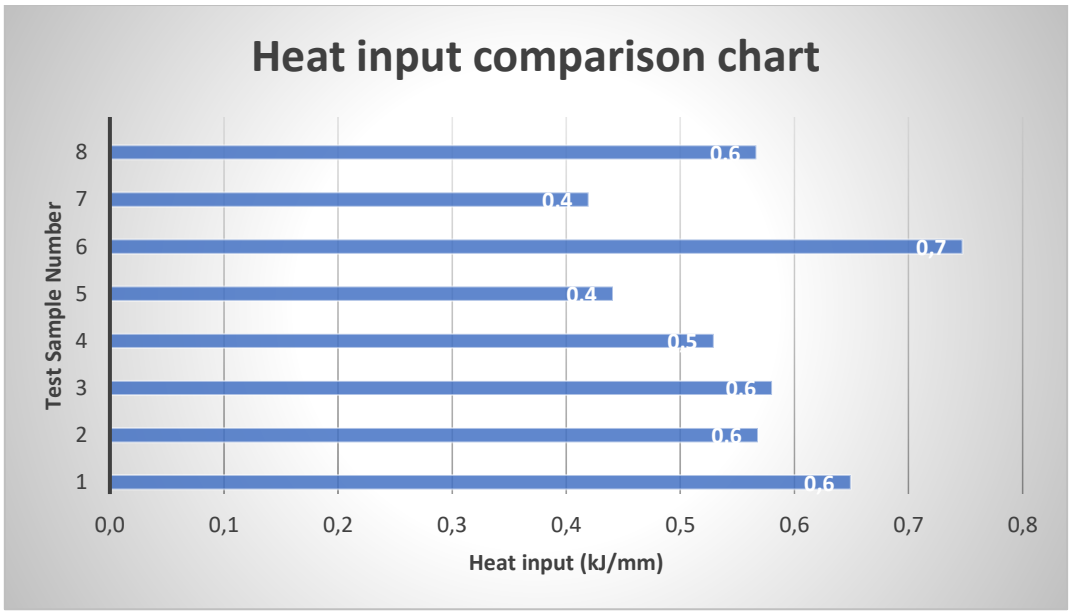

Figure 4-3: Comparison chart depicting difference in average heat input per sample.

4.1.2 Non-destructive testing

Non-fluorescent MT was performed on all test plates, before proceeding to laboratory testing. Each plate was tested for surface and subsurface defects. If defects were detected, the plates were re-welded and tested again. This ensured consistency in the successive laboratory results. All test plates were successfully welded and passed MT as shown in Figure 4-4. Sample 5 showed a defect free capping and root run.

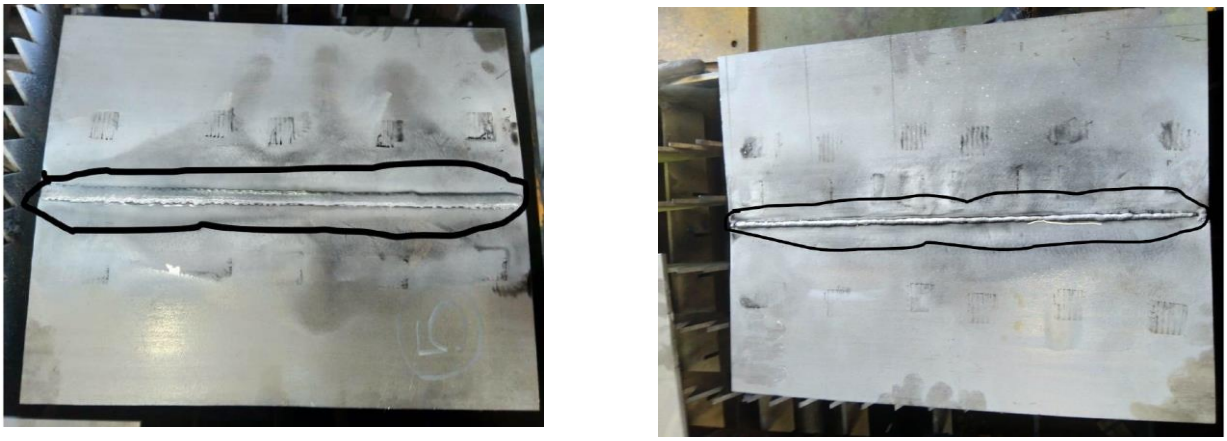

Figure 4-4: Encircled weld area after MT testing showing weld cap (left) and root run (right) of Sample 5.

4.2 Weld macro results and discussion

With the low ionisation potential of argon, the gas produces a constricted stable arc, and at high current density the arc is concentrated on one area causing a deep finger-like penetration in welds. Helium on the other hand, with a high ionisation potential, requires a high arc voltage implying a lower arc stability as compared to argon. This causes a broader and more shallow penetration pattern (Kou, 2003). The bead contours for pure argon and helium produced a broad but shallow penetration profile whilst pure argon produced a deeper finger-like penetration. Due to the difficulty experienced in welding with pure argon, due to an unstable arc, along with the wide range of defects, the gas was not studied in detail. Defects that were observed after multiple attempts to weld with pure argon included but were not limited to: (i) inconsistent root penetration; and (ii) lack of fusion. Argon was therefore not considered as a possible gas of choice for the welding of 3CR12 in the manufacturing of wagons. Further research found that the reason pure argon cannot be used in welding stainless steel is due to its low thermal conductivity and unstable arc. Due to the edges of the arc remaining relatively cool, reduced penetration and fusion is obtained. The reduced arc power (which is the result of the low ionisation potential) prevents the formation of a workable fluid puddle, making it difficult for

the welder to control the weld pool. These factors contribute to a poor-quality weld (Valiente Bermejo et al., 2015).

Table 4-2 depicts the macrostructures of samples that were fabricated from gases that produced visually acceptable welds. It was noted that a slight undercut was observed when using pure helium as the shielding gas. This, however, could be attributed to the high thermal conductivity of the gas and the skill of the welder. After several attempts the undercut defect was reduced to acceptable standards. With the addition of carbon dioxide or oxygen to argon, a larger fusion area of the root run is shown in the wide macrostructures of images 2, 3 and 6 and a more convex shape of weld was produced. The binary gas mixture of argon and helium shows a preferable shape in the capping run of the argon rich mixture as compared to the flat cover pass run obtained from the 50/50 composition as can be seen in images 5 and 7 in Table 4-2. It is however important to note that a variety of factors contribute to the shape of these welds, and that these will vary from welder to welder. These factors include the travel speed during welding, wire feed speed, torch distance and voltage and current (The Lincoln Electric Company, 2014).

Table 4-2: Macrostructures of samples 1-8 welded under various gas mixtures

Gas	***Sample No.***	***Macro***	***Gas***	***Sample No.***	***Macro***
He	1	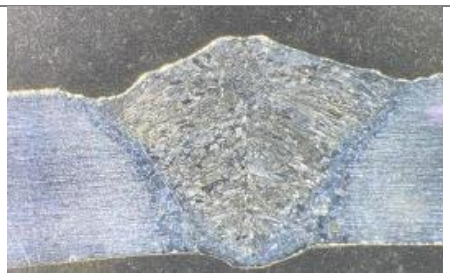	95Ar, 5CO_2	2	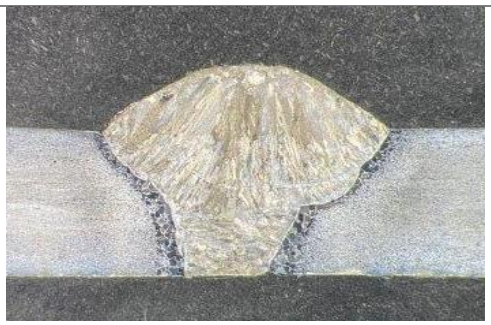
98 Ar, 2 CO_2	3	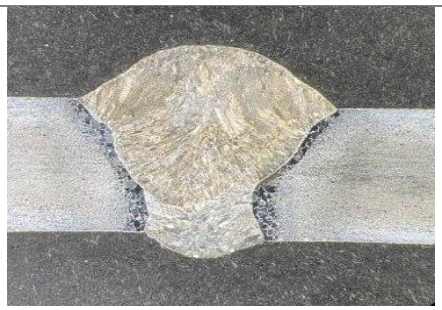	73Ar, 25He, 2CO_2	4	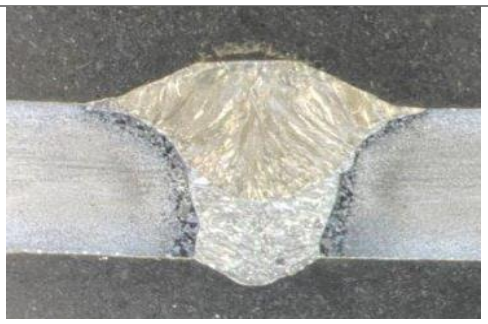
75Ar, 25He	5		98Ar, 2O_2	6	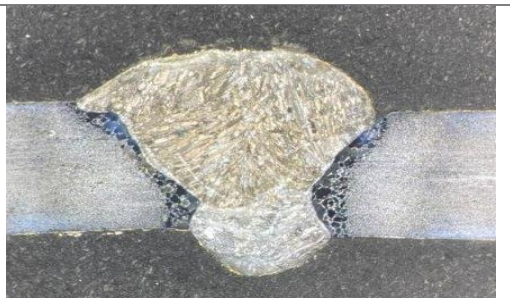
50Ar, 50He	7	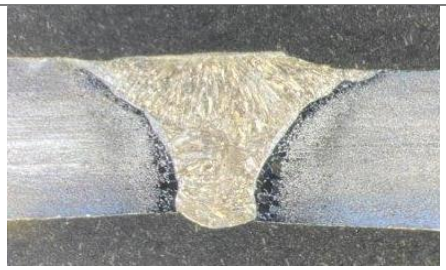	93Ar, 2O_2, 5CO_2	8	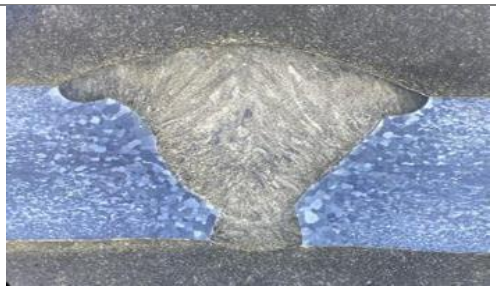

4.3. Mechanical Results

4.3.1. Tensile tests

The tensile test results are represented in Figure 4-5 and Table 4-3. Two samples were pulled for each test plate and an average determined for representation.

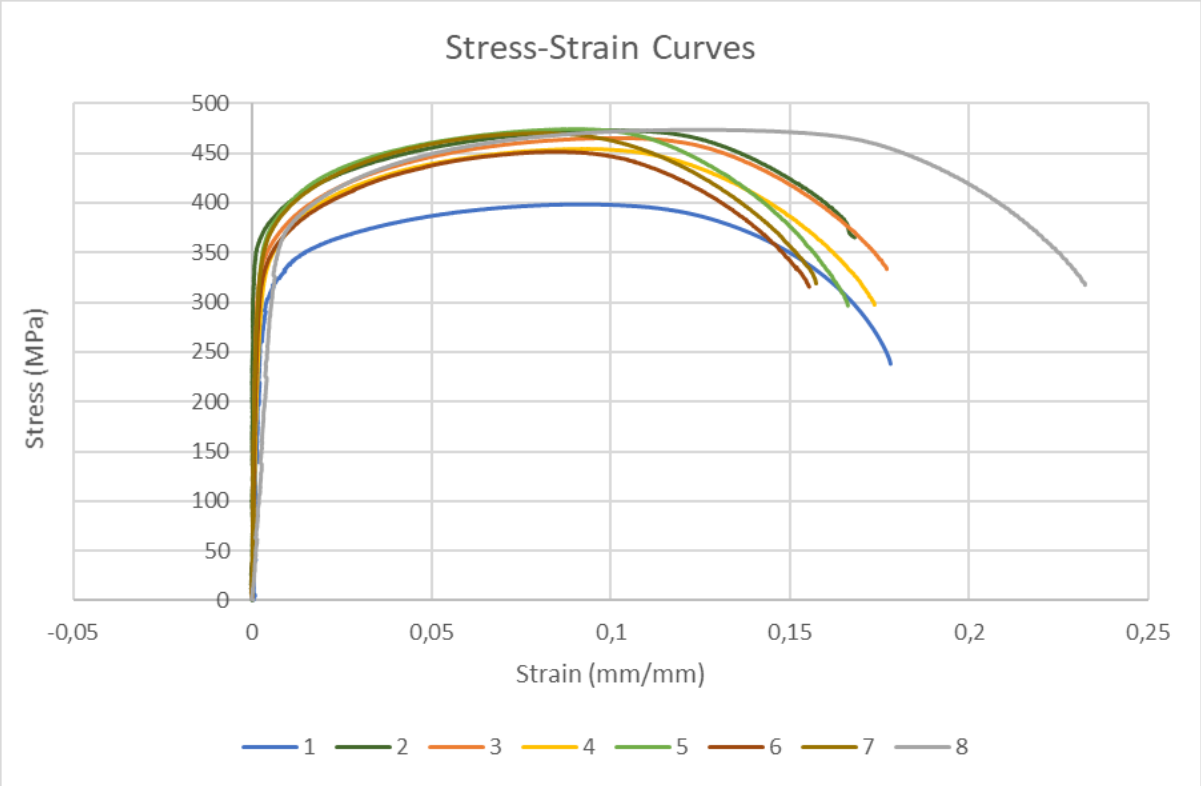

Figure 4-5: The stress – strain curve of the samples.

Table 4-3: Tabulated values of the tensile testing.

Properties	*Min values as per EN 10088-2*	*1*	*2*	*3*	*4*	*5*	*6*	*7*	*8*
Ultimate Tensile Strength (MPa)	450 min.	398	473	462	454	474	451	470	474
Yield Strength (MPa)	280 min.	307	371	341	337	362	336	355	362

All samples, apart from those welded under helium shielding gas, were above the ultimate tensile strength (UTS) specified by EN 10088-2 (British Standards Institution, 2014), and the

material certificate. Sample 1 (100%He) has a UTS of 398 MPa, which is well below the minimum requirement of 450 MPa as per EN 10088-2 standard, and although the sample shows an acceptable yield strength, this value is the lowest compared to the other specimens. In comparison, Sample 2 (95%Ar, 5%CO_2) and Sample 8 (93%Ar, 2%O_2, 5%CO_2) display the most impressive results.

From the results, it appears that by reducing the amount of CO_2 from 5% to 2% leads to a decrease in the yield and UTS of the weld. These results are not in agreement with information provided by the Lincoln Electric Company on the effects of adding CO_2 as a reactive gas, however, the results correspond with the study conducted by Anand et al, (2013), on the welding of 304L stainless steel in which higher tensile strength and hardness values were found in the weld compared to the base metal when there is an increase in the amount of CO2 in a shielding gas. This shows that shielding gases affects the properties of various materials in different ways and that the effects cannot be generalised. The difference on the UTS and yield strength of the welds when adding O_2 or CO_2 is very minimal, as can be seen in Sample 3 and Sample 6. The same is true for the helium/argon gas ratio in Samples 5 and Sample 7. However, when comparing Sample 4 and Sample 5, the results show that by adding CO_2 to a helium and argon blend increases the UTS and yield strength of the welded specimen.

4.3.2. Charpy Impact Testing

Impact testing was performed at room temperature (23°C), -20°C and -7°C on the 8 samples. The DBTT curve for impact tests is shown in Figure 4-6 and the data is shown in Table 4-4

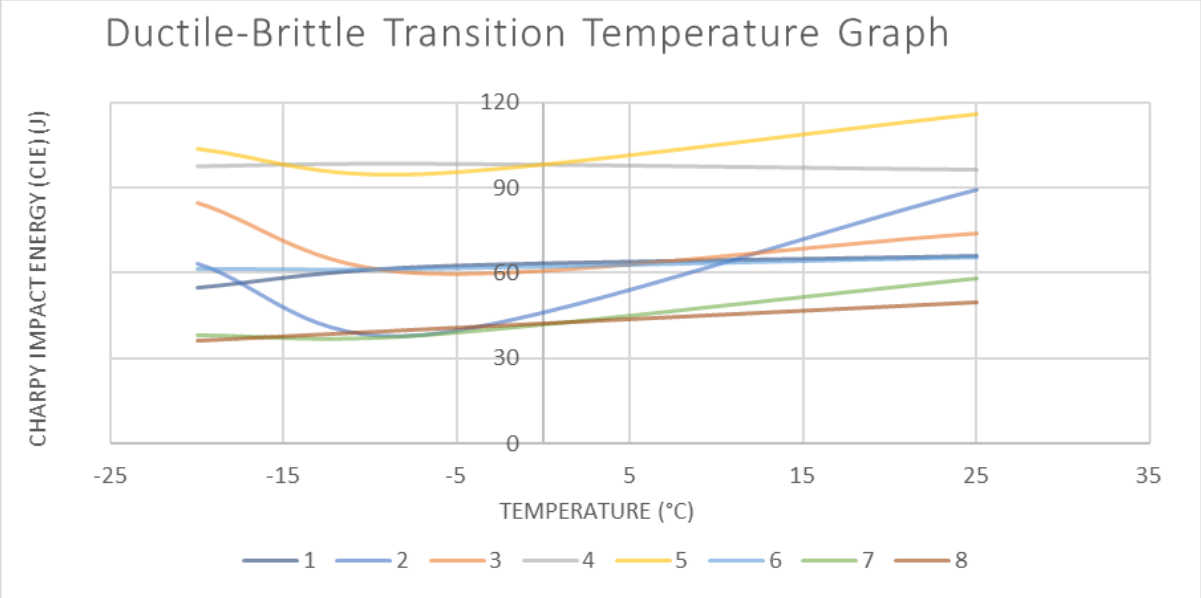

Figure 4-6: The DBTT graph of the welds.

Table 4-4: Tabulated average values of the impact testing the various welded samples

Properties	*Temperature*	*3CR12 Columbus stainless steel data sheet*	*1*	*2*	*3*	*4*	*5*	*6*	*7*	*8*
Charpy impact energy (J)										
	-20°C	35 min	55	63	85	98	104	61	38	36
	-7°C		62	38	60	99	95	61	38	40
	25°C		66	89	74	96	116	65	58	50

All samples presented impact energies above the minimum specified value of 35J. Sample 7 (50Ar/ 50He) provided the lowest impact values followed closely by Sample 8 (93Ar, $2O_2$, $5CO_2$). Sample 4 and Sample 5 with the 25% He composition showed the highest impact values suggesting that a helium in a smaller ratio significantly improves the ductility of the weld. The improved toughness values by the 75/25 argon/helium mixture agree with the studies by

Valiente Bermejo et al., (2015), who found that gas mixtures containing helium had higher ductility and impact values than samples containing argon and CO_2. In this study the same was found between Samples 2, 3 and 5.

It can also be deduced from the results that reducing the amount of CO_2 in the shielding gas results in an increase in toughness, as can be seen in Samples 2 and 3, at lower temperatures. However, the samples show a decrease in toughness with a reduction in CO_2 at room temperature. The increase in toughness with corresponding reduction in CO_2 at temperatures below freezing temperatures correspond with findings by Kah and Martikainen (2012). However, the data presented in the study by Kah and Martikainen (2012) did not include impact studies at temperatures above -20 °C.

4.3.3. Micro-hardness testing

The micro-Vickers hardness testing was performed on the samples with indentations taken 1 mm apart from the substrate, through the HAZ and the weld, to the other side of the weld. The data was processed to draw a hardness profile as shown in Figure 4-7.

The 3CR12 Columbus stainless data sheet specifies a maximum of 225 HV. To analyse the values in more detail the average hardness values are tabulated as shown in Table 4-5.

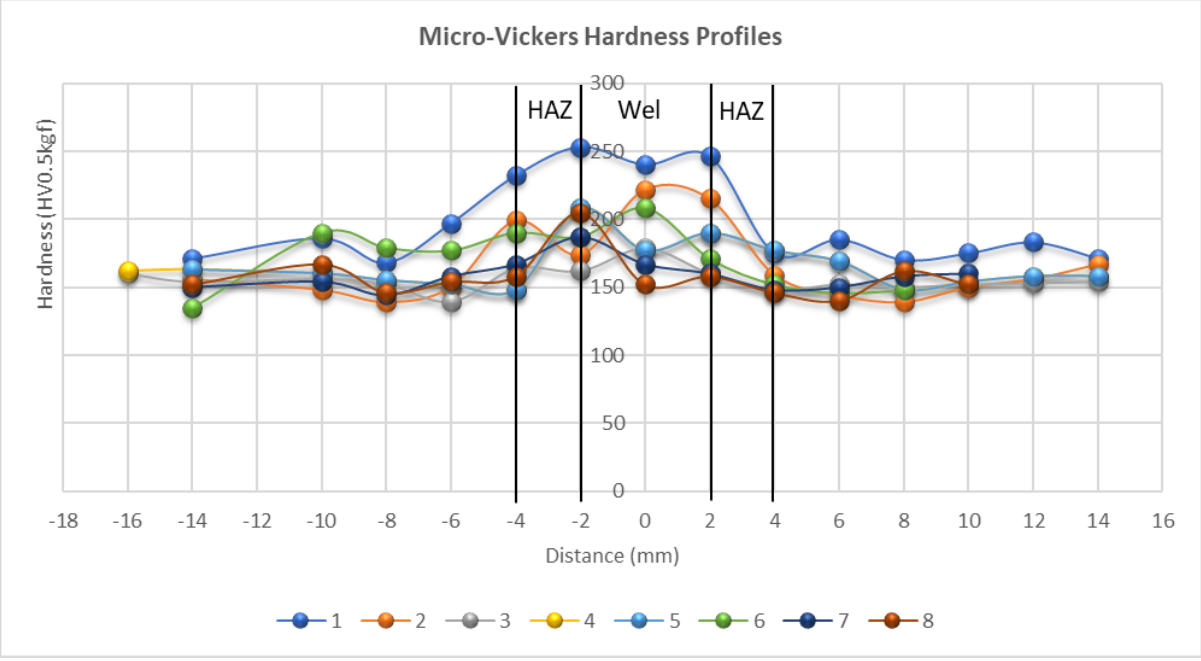

Figure 4-7: The micro-hardness profile of the tested welds.

Table 4-5: Average hardness (in HV) of the different weld zones

Zone	*1*	*2*	*3*	*4*	*5*	*6*	*7*	*8*
Parent	178.0	154.8	155.3	153.5	157.0	146.0	155.3	172.0
HAZ	205.5	146.2	148.0	143.5	148.0	162.0	152.5	151.7
Weld	228.3	202.5	182.8	166.3	184.2	188.2	173.7	199.9

Ferritic structures are softer than austenitic structures as proven by the weld hardness profiles that were obtained. The welds have higher hardness values than the parent material. High hardness in the HAZ is due to martensite that forms along grain boundaries, whilst the high hardness in the weld is attributed to the austenitic structure. From the graph presented in Figure 4-7, the average hardness is highest in the weld and lowest in the parent metal. The hardness profile does not show a linear increase from the parent material to the weld. This is because microhardness can indent specific phases. Hence within the HAZ, the indentations with high hardness values are most likely due to the formation of martensite whilst those with lower hardness show the ferrite phases. Apart from the average hardness value in the weld area of Sample 1 (100% He) being slightly higher at 228.3 HV (shown in red), the remainder of the values fall within an acceptable range.

The amount of CO_2 has an effect on the carbon content in the weld, which determines hardness. From the study, it was noted that the hardness values decreased with an increase in CO2 content. Similar behaviour was reported by Kah and Martikainen (2012). It can also be deduced that adding either CO_2 or O_2, to argon in equal ratios has no significant effect on the hardness of the material. The addition of both reactive gases to argon (Sample 8), does however increase the hardness of the weld metal and heat affected zone significantly.

4.4. Phase and microstructural analysis

The parent material taken at 10× magnification shows a fully ferritic microstructure, and this is attributed to the low carbon content in 3CR12 as depicted in Figure 4-8. The microstructure of the weld metal can be explained by the Schaeffer diagram using the chemical composition of both the base and filler metal. This is found by calculating the nickel equivalent (Ni_{eq}) and chromium equivalent (Cr_{eq}) of the parent metal and the filler metal using Equations 4- 2 and 4-3. The Ni_{eq} and the Cr_{eq} values used are shown in Table 4-6 (Kotecki and Siewert, 1992).

Figure 4-8: Microstructure of the 3CR12 parent material.

$$Ni_{eq} = \%Ni + 30\,x\,\%C + 0.5\,x\,\%Mn$$ ……...Equation 4-2

$$Cr_{eq} = \%Cr + \%Mo + 1.5\,x\,\%Si + 0.5\,x\,\%Nb + 2\,x\,\%Ti$$ …… Equation 4-3

Table 4-6: Ni_{eq} and Cr_{eq} of the alloys used in this experiment.

Materials	*3CR12*	*AISI 308*
Ni_{eq}	1.36	10.85
Cr_{eq}	12.73	20.20

The location of various alloys on the Schaeffler diagram are indicated in Figure 4-9. The red dots represent the expected microstructure for the ER308L filler wire material and the 3CR12 base metal. The 3CR12 is positioned in the martensite and ferrite area whilst the ER308L electrode has a structure which consists of approximately 8% ferrite and 92% austenite. The red tie line represents how the structure will vary with different dilutions of the filler metal. Albuquerque et al., (2009), advises that the dilution percentage is between 20%-40% for most frequent welding processes. In a study by Luijan et al., (2020), it was found that when welding low carbon steel to 3CR12 with ER308L wire, the dilution of the base metal was 24% at similar welding parameters used in this study. At 24% dilution, the weld metal should consist of a mixture of austenite, martensite, and ferrite as depicted by the blue arrow in Figure 4-9.

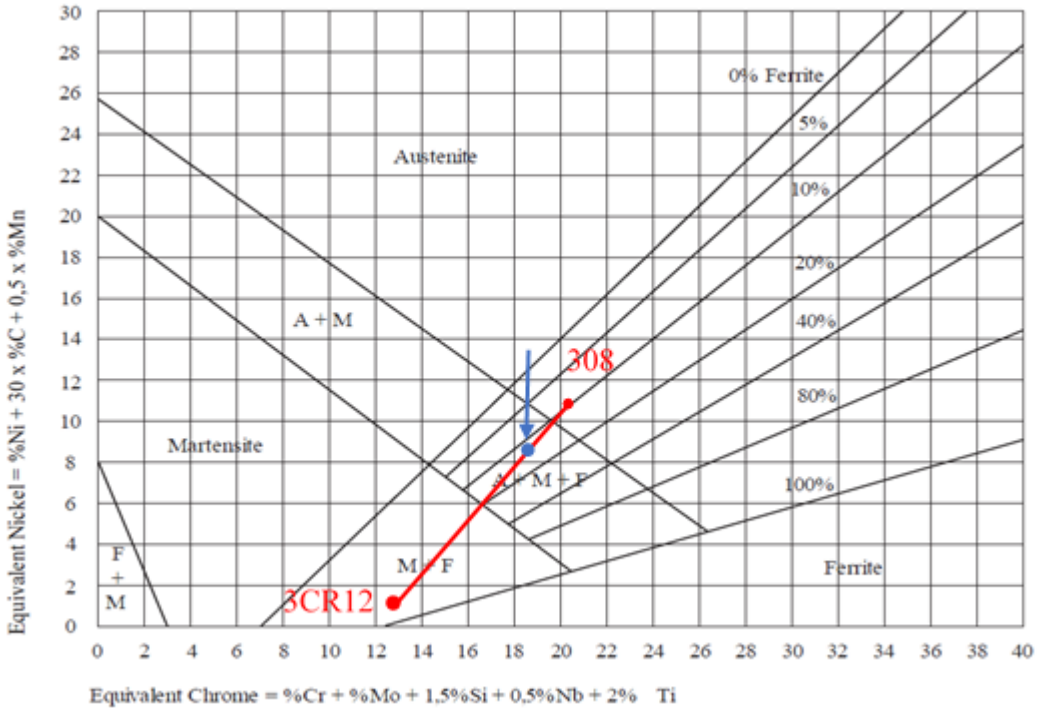

Figure 4-9: Schaeffler diagram depicting the expected phases

Figure 4-10 shows the HAZ and weld microstructures of the 8 samples taken at 10X magnification. The microstructure of the HAZ adjacent to the weld interface or fusion line after cooling showed excessive grain growth which consisted of α ferrite with islands containing martensite (i.e., grain boundary martensite) on Samples 1 to 8. Martensite forms because of high cooling rates associated with welding. High cooling rates prevent the transformation of austenite to ferrite at lower temperature and any austenite formed during cooling will transforms to low carbon martensite (Balsaraf *et al.*, 2013)

Samples 1, 4, 5, 6 and 7 show substantially less martensite in the HAZ when compared to Samples 2, 3 and 8. This could be attributed to the presence of helium as the shielding gas. According to Kah and Martikainen (2012), an increase in CO_2 in the shielding gas leads to an increase in carbon in the weld metal which increases the amount of martensite formed at the grain boundaries. The results clearly show the relationship between CO_2, carbon, and hardenability in the weld. All welds show similar microstructures consisting of austenite, and interdendritic ferrite. The phase compositions of the welds were further investigated using XRD analysis.

	HAZ	*Weld*
1	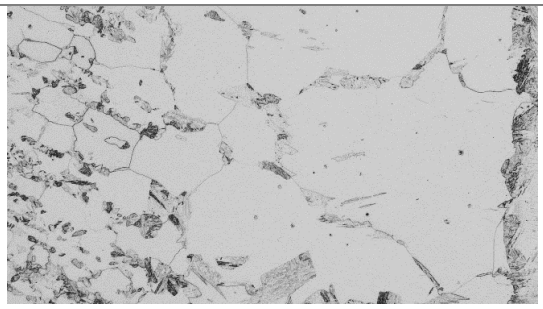	
2	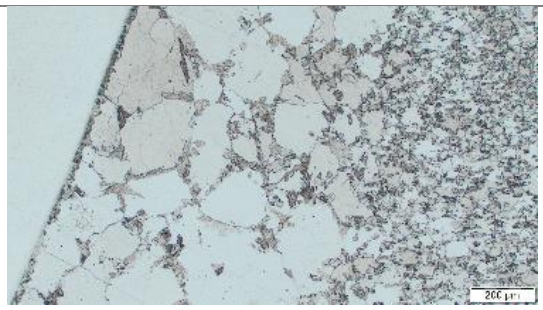	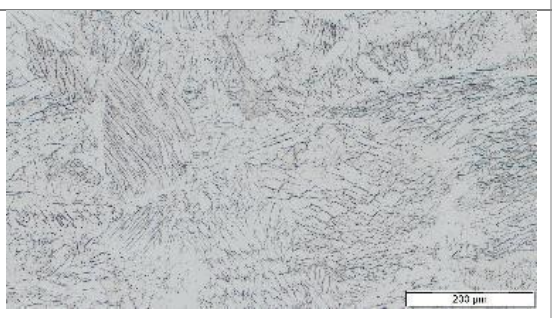
3	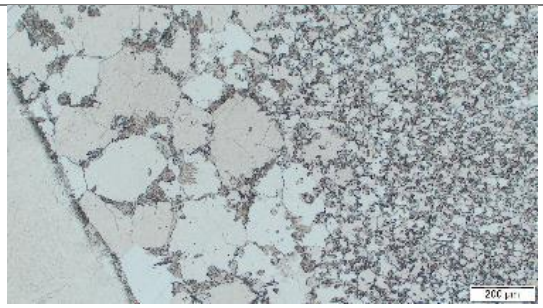	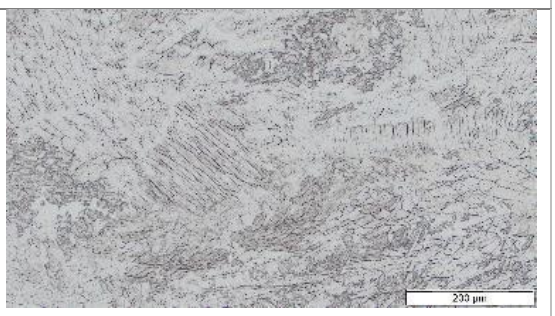
4	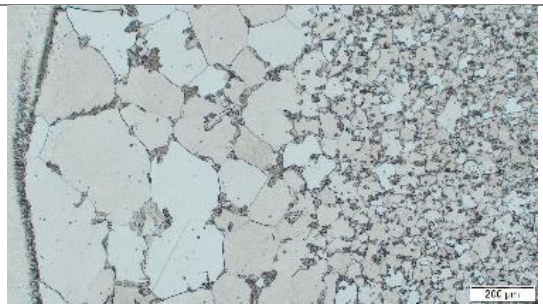	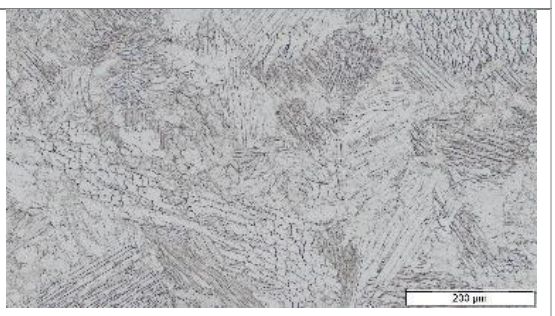
5	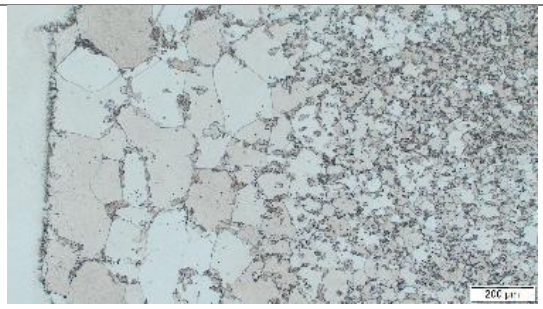	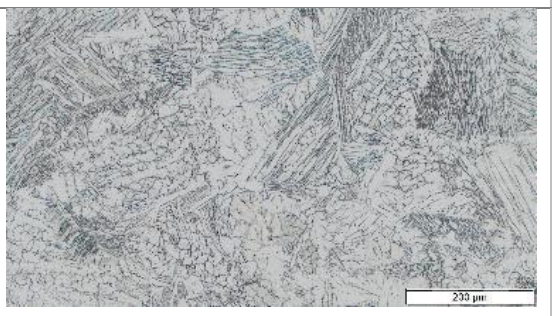

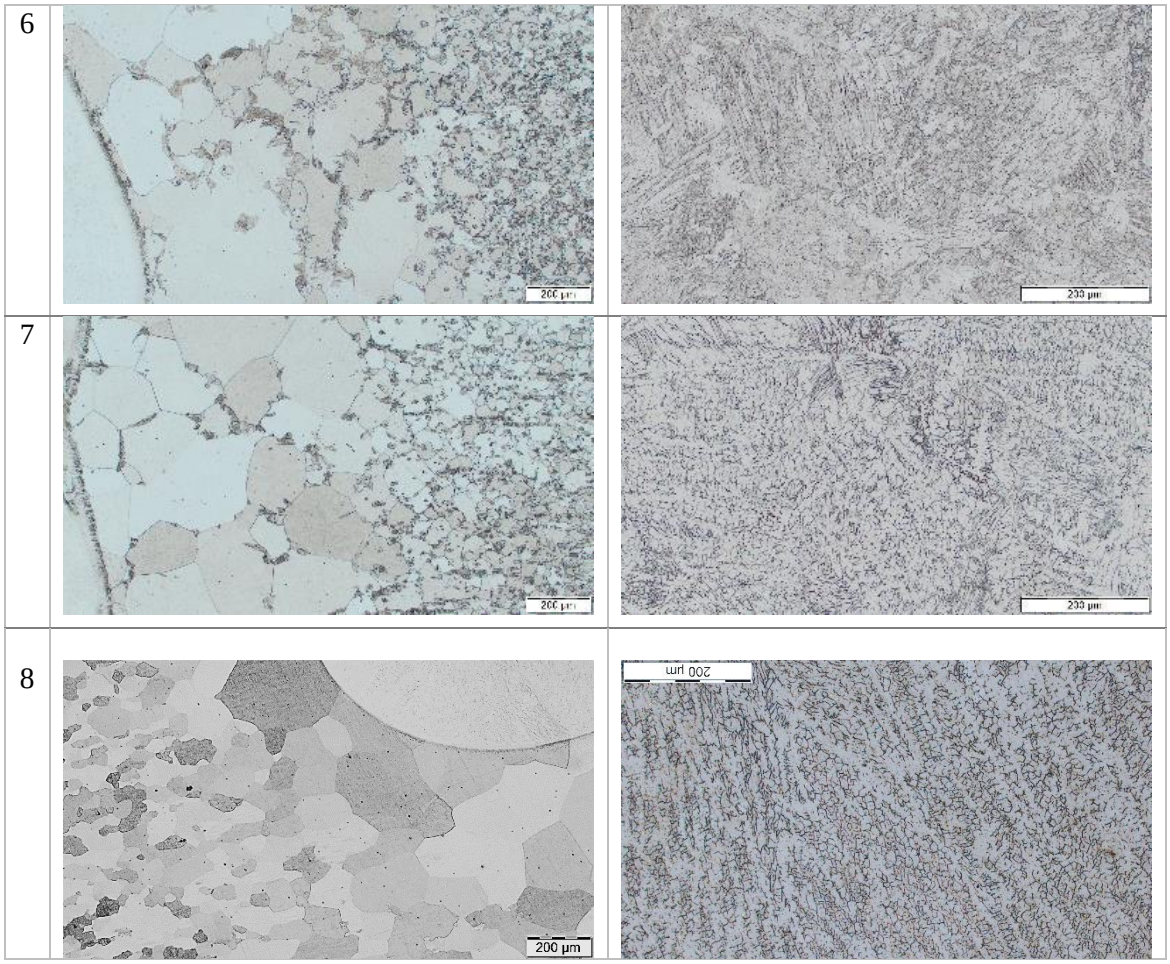

Figure 4-10: Microstructures of gas metal arc welded samples produced by varying shielding gases

The results of the XRD analysis completed on the welds show the percentage of austenite relative to ferrite in Table 4-7. Sample 1 (He) has the most ferrite in contrast to Sample 5 (75% Ar, 25% He) which contains the least amount of ferrite. The average ferrite content was estimated to be around 12% from the Schaeffler diagram. A proper amount of ferrite in the weld metal is essential as the ferrite structure inhibits hot cracks in the weld metal. This is because ferrite can dissolve harmful elements such as sulphur and phosphorus which can segregate to the weld metal and increase the risk of cracks when residual stresses increase. Kou (2003), has shown that weld metal containing between 2%-10 % ferrite structures in a stainless-steel weld metal is desirable. Anything above 10% will reduce the corrosion resistance of the weld. The ferrite content for Samples 2 (95%Ar, 5%CO_2), 4 (73%Ar, 25%He, 2%CO_2) and Sample 5 (75%Ar, 25%He) were found to be acceptable. In a study by Liao and Chen (1998), it was found that the volume fraction of ferrite decreases as the amount of CO_2 in the shielding gas increases. This is apparent in the ferrite content of Samples 2 and 3 which contain 5% and 2% CO_2 respectively.

Although no information is available on the effect of helium or argon on the. microstructural properties of welds, it can be shown that helium on its own, promotes a high ferrite content in weld metal. By adding argon to this mixture, the ferrite content is reduced as can be seen when comparing Samples 5 and Sample 7 which contain 75% and 50% argon respectively.

Table 4-7: Percentages of the phases found in the various gas samples.

Phase	*Percentage (%)*							
	1	*2*	*3*	*4*	*5*	*6*	*7*	*8*
Austenite	80.4	95.7	85.6	95.1	96.1	89.7	87.5	88
Ferrite	19.6	4.3	14.3	4.9	3.9	10.3	12.5	12

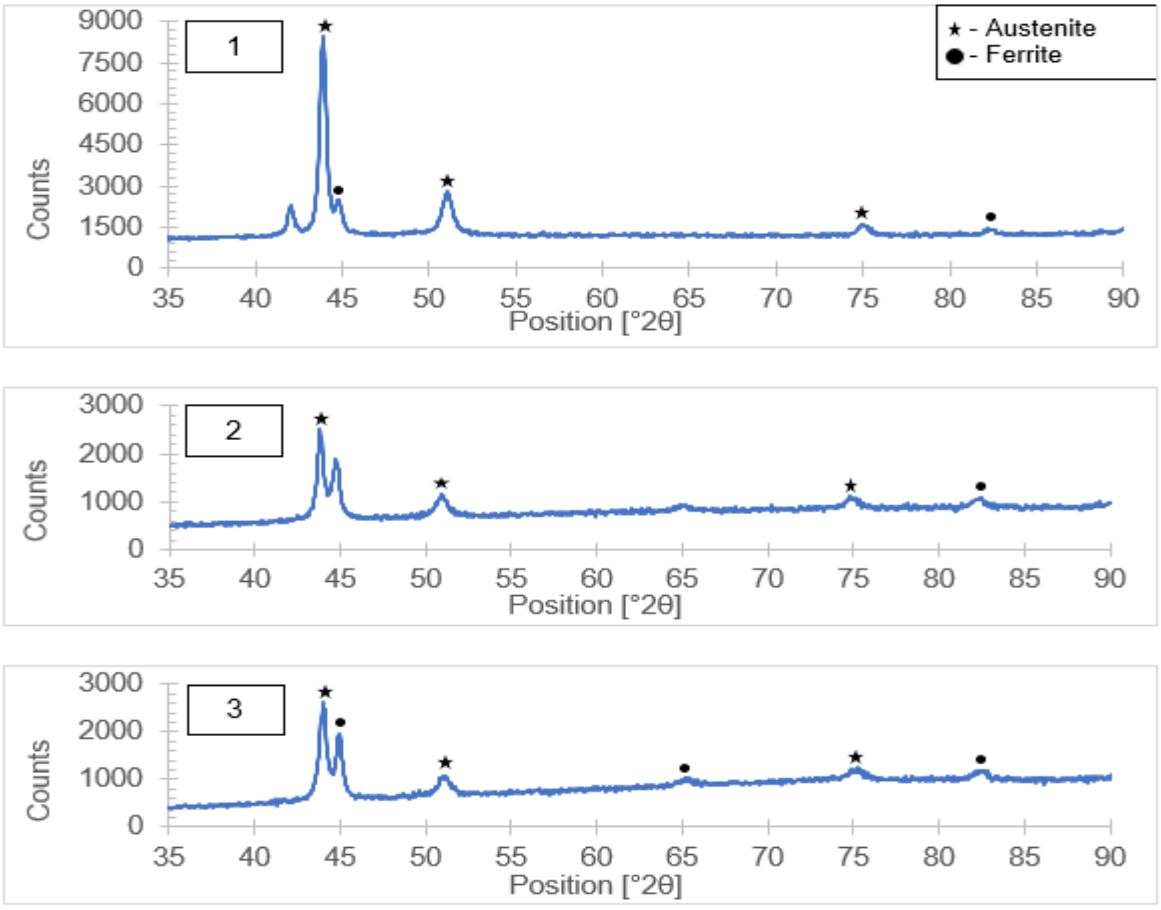

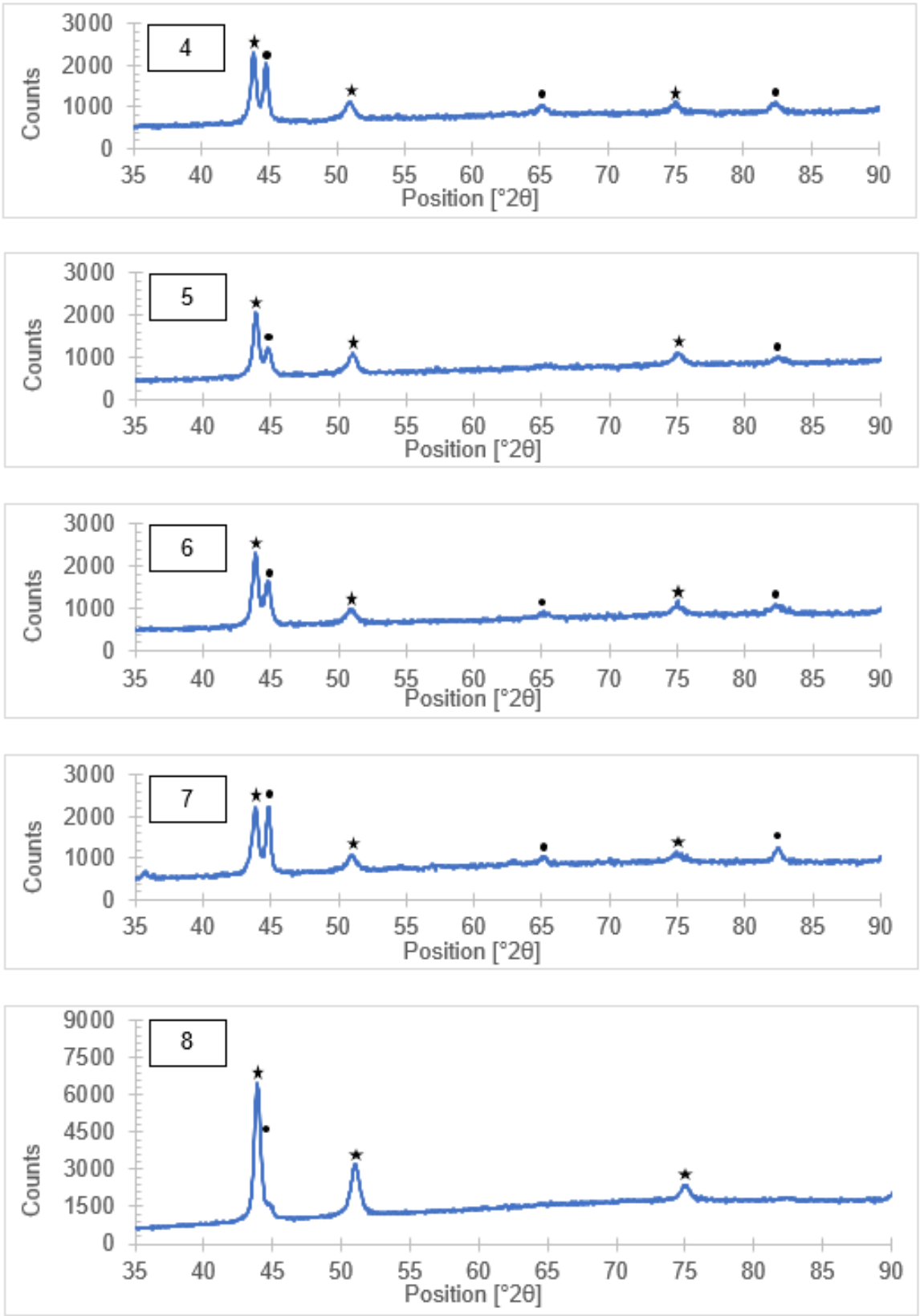

Figure 4-11: Diffractogram results of the XRD analysis for samples 1-8.

4.5. **Sensitisation results and discussion**

The Strauss test was used to test for sensitisation in the HAZ region. Sample 1(He) and Sample 2 (95%Ar, 5%CO_2) showed visible signs of sensitisation as seen in Figure 4-12. Looking at the sensitisation for Sample 2 at a higher magnification, it is evident that the grain boundaries are corroded whilst Sample 1 shows ditched grain boundaries. The electro-etching, however, did not reveal any sensitisation in any sample. Figure 4-13 is a representation of what was found in the electro-etched samples.

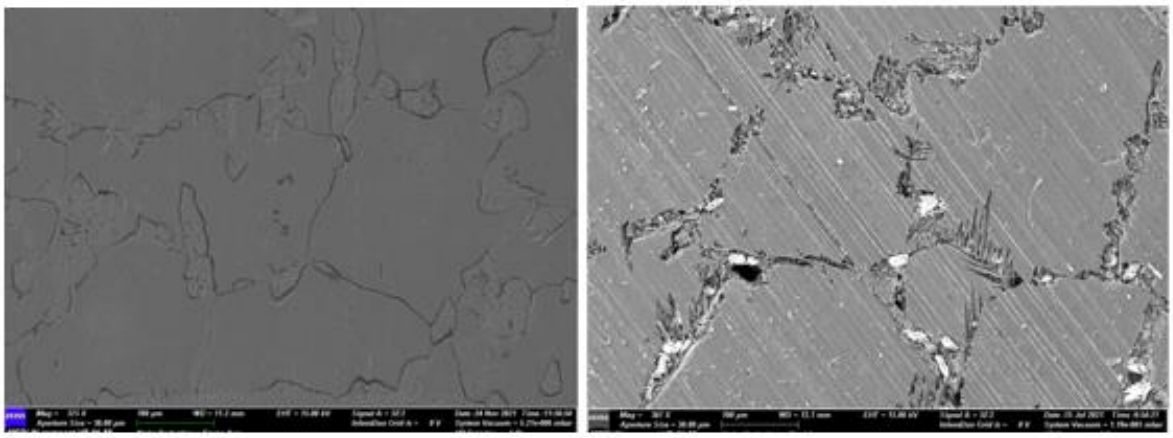

Figure 4-12: SEM images from STRAUSS test showing sensitisation in Samples 1 and 2.

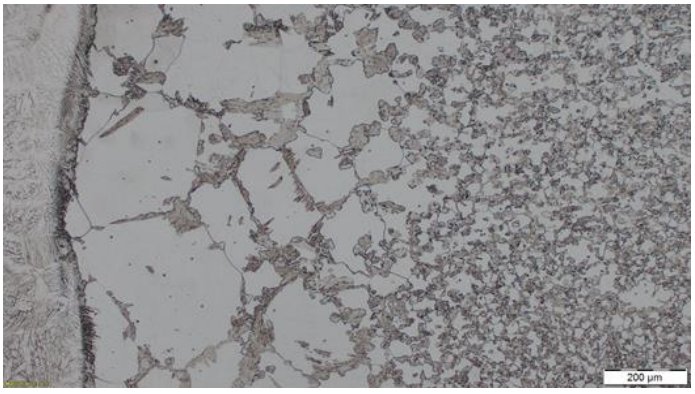

Figure 4-13: HAZ of sample 2 after electro-etching.

Although Columbus Steel (2007) recommends a heat input range of 0.5kJ/mm to 1.5kJ/mm to avoid sensitisation, it is evident that keeping within this range does not eliminate sensitisation when applying various shielding gases. Dahmen et al. (2015), goes on to mention that the formation of martensite eliminates the ferrite-ferrite grain boundaries at the HTHAZ, which in turn prevents sensitisation, however in this study, martensite was found on both samples 1 and 2. This leaves room for further investigation on the effects of various gases on the sensitisation behaviour of 3CR12.

4.6. Summary

A summary of the test is shown in Table 4-8, presenting the samples with acceptable results according to BS EN 10088-2 and literature. The macrostructures of all welds showed defect free welds for all gas mixtures according to EN ISO 5817:2014. However, the helium gas showed to be slightly problematic, forming discontinuities that can be detrimental to the overall performance of the weld. In addition, the pure helium shielding gas (Sample 1), failed the Strauss test for sensitisation and is therefore not considered for the welding of 3CR12 in this study. Acceptable welds were produced for the remainder various gas mixtures and studied in detail.

The microstructures revealed good weld quality. All weld metal revealed similar austenitic structures with interdendritic ferrite. The HAZ of samples 1 to 7 displayed α ferrite with islands of martensite whilst sample 8 showed grain growth of α ferrite only. It was observed that increasing carbon dioxide induced less martensite on the grain boundaries of Samples 2 and 3 with CO_2 concentration of 5% and 2%, respectively. Carbon dioxide also forms smaller grains compared to oxygen when using argon as the base gas. These can be seen in images 3 and 6 in Figure 4-10. CO_2 in higher quantities caused sensitisation on the weld (Sample 2), rendering this mixture unacceptable.

Although pure helium was initially difficult to weld and caused sensitisation, mixing the gas with argon yielded better results. However, a smaller ratio of helium to argon should be used due to loss of ductility in the 50/50 mixture. Sample 4 and Sample 5 with a lower helium content of 25%, showed high impact values. The higher impact strength found in the samples could be attributed to the lower ferrite in the weld.

Finally, Sample 8 which is generally used in welding 3CR12 showed favourable results in most tests apart from the impact testing. The results for this tri-mixture were above the minimum value of 35J however the gas demonstrated the lowest impact values at all temperatures when compared to gas mixtures 1 to 7.

Table 4-8: Summary of acceptable results (represented by x) per test sample.

Test No.	*Gas*	*Microstructures*	*XRD*	*Tensile*	*Hardness*	*Impact*	*Sensitisation*
1	He	x				x	
2	95%Ar, 5%CO_2	x	x	x	x	x	
3	98% Ar, 2% CO_2	x		x	x	x	x
4	73 Ar, 25He, 2CO_2	x	x	x	x	x	x
5	75 Ar, 25He	x	x	x	x	x	x
6	98Ar, 2O_2	x			x	x	x
7	50Ar, 50He	x			x	x	x
8	93Ar, 2O_2, 5CO_2	x		x	x	x	x

5. CHAPTER 5

CONCLUSION AND RECOMMENDATIONS

The aim of this research was to determine the effects of various mixtures of Ar, He, O_2 and CO_2 on the strength, toughness, hardness, corrosion resistance and metallurgical properties of 3CR12 when welded with ER308L wire. The gas mixture that produced superior mechanical and metallurgical properties was determined through the welding of 6 mm 3CR12 plates with ER308L wire using pure Ar and He gas, and various gas mixtures of Ar, He, O_2 and CO_2. Non-destructive tests using visual and magnetic particle inspection were conducted to evaluate surface quality of the welds and microstructural properties were determined using the optical microscope, scanning electron microscope and XRD for phase analyses. Mechanical properties such as fracture toughness, ductility, and ultimate tensile strength were also successfully examined collectively with the corrosion performance of each weld joint.

5.1. Conclusions

The effects of pure helium, argon, and mixtures of these gases on the bead contours and penetration were studied in detail. Whilst pure helium produced slight undercuts, a 25% mixture of the gas with argon and CO_2 showed good root penetration and bead contour (Sample 4). He when mixed with argon in binary (25/75) and without CO_2 (Sample 5), shows a good bead profile, however the root penetration was shallower than Sample 4. Adding either CO_2 or O_2 to the gas mixtures resulted in larger fusion areas and a wider microstructure.

The welding voltage and current used during this research ranged between 20V to 22V and 100A to 150A, respectively. For these welds, the voltage, and current ranges together with the travel speeds, produced heat inputs below 1 kJ/mm, within the range 0.4-0.9 kJ/mm. The voltage range was in exception to the helium shielding gas which required a higher voltage of 28V to produce a sound weld. With the higher voltage, helium permits a higher travel speed and lower heat input. It was also evident that by increasing the amount of CO_2 in an argon binary blend, faster travel speeds were possible as compared to adding O_2.

The results show significant differences between the various gas ratios that were used in terms of microstructures, mechanical properties, and sensitisation. Although Sample 2 passed most of the tests, the sample, using 95%Ar/5%CO_2, failed the Strauss test and cannot be

recommended for further use. Sample 4 containing, 73% Ar, 2% CO_2, 25% He and Sample 5 containing, 75% Ar and 25% He (highlighted in Table 4-9), would be the possible recommendation for gas ratios due to the gases having better Charpy impact test results, low ferrite content, good tensile results, and no sensitisation. Due to the excellent weld bead profile and root penetration of Sample 4 however, this gas mixture would be recommended.

5.2. Recommendations

Future work would consist of in-service testing of the 73% Ar, 2% CO_2, 25% He gas mixture by welding a 3CR12 wagon using ER308L welding wire. Exposing these welds to the natural operating environment would provide more insight into the performance and lifespan of the wagons. Regular visual inspection of the wagon will be required together with annual NDT to confirm the presence or absence of discontinuities and defects. There is also room for the study of the remaining gases in terms of sensitisation in order to understand exactly how and why these gases cause this phenomenon when welding 3CR12 at the same parameters and heat inputs used for the gases that do not cause sensitisation.

6. APPENDIX A

TABLES FROM RESEARCH

Table A-1: Mechanical properties of 3CR12 (Columbus Stainless, 2007).

Type	Product Form[1] or Gauge (mm)	0.2% Proof Stress (MPa)	Tensile Strength (MPa)	Elongation (%)	Brinell Hardness	Impact Energy (J)
3CR12	<3	280 450	460 min	18 min[2]	220 max	
	3 to 4.5	300 450	460 min	18 min[2]	220 max	35[4]
	>4.5 to 12	300 450	460 min	20 min[2]	220 max	35[4]
	>12	300 450	460 min	20 min[2]	250 max	35[4]

Table A-2: Chemical composition of 3CR12 and similar ASTM and EN specified stainless steels (Columbus Stainless, 2007).

Type	*% C*	*% Si*	*% Mn*	*% P*	*% S*	*% Cr*	*% Ni*	*% N*	*% Ti*
3CR12	0.030 max	1.00 max	2.00 max	0.040 max	0.030 max	10.50 12.50	1.50 max		4(C+N) 0.6
1.4003	0.030 max	1.00 max	1.50 max	0.040 max	0.015 max	10.50 12.50	0.30 1.00	0.030 max	

Table A-3: Welding shielding gas characteristics (Kah and Martikainen, 2012)

Type of gas	*Content in air (vol%)*	*Boiling point at 1.013 bar (°C)*	*Atomic weight and mean molecular weight*	*Density at 15°C, 1 bar (kg m^{-3})*	*Relative density with regard to air (=1) at 15 °C*	*Dissociation and ionisation energies (eV)*[a]	*Chemical activity*
Hydrogen (H_2)	0.5×10^{-6}[b]	−252.9	2.016	0.085	0.06	4.84 13.59 -	Reducing
Argon (Ar)	0.934	−185.9	39.948	1.669	1.38	- 15.76 27.50	Inert
Helium (He)	5.2×10^{-6}[b]	−268.9	4.002	0.167	0.14	- 24.56 54.10	Inert
Nitrogen (N_2)	78.084	−195.8	28.013	1.170	0.91	9.76 14.55 29.60	Reactive
Carbon dioxide (CO_2)	0.033[b]	−78.5[c]	44.011	1.849	1.44	5.80 13.62 35.20	Oxidising Oxidising
Oxygen (O_2)	20.946	−183.0	31.998	1.337	1.04		

[a] 1 eV01.6×10−6 J; ionisation energy of most metal ranges between 6 and 9 eV

[b] Not obtained from the atmosphere

[c] Sublimation temperature

7. REFERENCES

Afrox (2018) *Product reference manual*. Available at: http://www.afrox.co.za/en/images/2018 Product Reference Manual full_tcm266-576594.pdf (Accessed: 5 November 2019).

Albuquerque, D., Tavares, J.M.R.S. and Cortez, P.C. (2009) 'Measurement of Welding Dilution from Images Using Active Contours', *Image Processing*, (June), pp. 22–24. Available at: https://www.researchgate.net/publication/258031843_MEASUREMENT_OF_WELDING_DILUTION_FROM_IMAGES_USING_ACTIVE_CONTOURS (Accessed: 15 February 2022).

American Society for Testing and Materials (2004) *ASTM A240: Standard Specification for Chromium and Chromium-Nickel Stainless Steel Plate, Sheet, and Strip for Pressure Vessels and for General Applications, ASTM International*. Available at: https://www.academia.edu/ (Accessed: 11 February 2020).

Amuda, M.O.H. and Mridha, S. (2011) 'An overview of sensitization dynamics in ferritic stainless-steel welds', *International Journal of Corrosion*, 2011. doi:10.1155/2011/305793.

Anand, N.R., Vijaysingh, M.C. and Nitin, K.S. (2013) 'The effect of shielding gases on mechanical properties and microstructure of austenitic stainless-steel weldments', *International Journal of Mechanical Engineering and Robotics Research*, 2(4), pp. 253–262. doi:1 September 2020.

ASTM International (2004) *Standard Practices for Detecting Susceptibility to Intergranular Attack in Ferritic*. United States of America.

ASTM International (2013) *Standard Test Methods for Tension Testing of Metallic Materials*. United States of America. doi:10.1520/E0008_E0008M-13A.

Balsaraf, D. D., S. P. Ambade, A. Patil, and Y. M. Puri. (2013) 'Literature Review on Analysis of Sensitization and Corrosion of Ferritic Stainless Steel (FSS) by Different Welding Processes', *International Journal of Advanced Materials Manufacturing and Characterization*, 3(1), pp. 263–268. doi:10.11127/ijammc.2013.02.048.

British Standards Institution (2011) 'BS EN ISO 9015- Destructive tests on welds in metallic materials — Hardness testing Part 1: Hardness test on arc welded joints.

British Standards Institution (2014) *BS10088-2: Stainless steels Part 2: Technical delivery conditions for sheet/plate and strip of corrosion resisting steels for general purposes*. British Standards Online.

British Standards Institution (2017) *BS14343: Welding consumables — Wire electrodes, strip electrodes, wires, and rods for arc welding of stainless and heat resisting steels — Classification*. British Standards Online.

Campbell, S.W., Galloway, A. and Mcpherson, N.A. (2012) 'Techno-economic evaluation of reducing shielding gas consumption in GMAW whilst maintaining weld quality', *The International Journal of Advanced Manufacturing Technology* [Preprint], (December). doi:10.1007/s00170-012-3961-2.

Collen, A. (2015) *3CR12 In action*. doi:10.1037/14665-002.

Columbus Stainless (2007) *Technical data 3CR12, 3CR12L, CS410S*. Available at: https://sassda.co.za/ (Accessed: 22 October 2019).

Dahmen, M., Rajendran, K.D. and Lindner, S. (2015) 'Sensitization of Laser-beam Welded Martensitic Stainless Steels', *Physics Procedia*, 78(August), pp. 240–246. doi: 10.1016/j.phpro.2015.11.034.

Deepak, J. R., V. K. Bupesh Raja, P. Viswanatha Reddy, L. Lakshmi Venkata Sai, and G. Ashok Kumar Reddy. (2019) 'Investigation of microstructural and metallurgical properties of Corten A588 grade steel GTAW joints', *International Journal of Mechanical and Production Engineering Research and Development*, 9(5), pp. 1257–1264. doi:10.24247/ijmperdoct2019111.

Doerr, C., Kim, J. and Jacobs, L.J. (2017) 'Evaluation of Sensitization in AISI 304 and AISI 304L Stainless Steel with Nonlinear Ultrasonic Rayleigh Wave Measurements', *NDT & E International*, 88, pp. 17–23. doi: https://doi.org/10.1016/j.ndteint.2017.02.007.

Dománková, M., Kocsisová, E. and Slatkovský, I. (2014) 'The microstructure evolution and its effect on corrosion properties of 18Cr- The Microstructure Evolution and Its Effect on Corrosion Properties of 18Cr-12Ni-2, 5Mo Steel Annealed at 500- 900°C', *Acta Polytechnica Hungarica*, 11(3), pp. 125–137. Available at: http://acta.uni-obuda.hu/Domankova_Kocsisova_Slatkovsky_Pinke_49.pdf.

Engineering News (2012) 'Company Announcement: 3CR12 Reaches One Million Tonnes Milestone', *Engineering News*, May, pp. 3–6. Available at: https://www.engineeringnews.co.za/article/company-announcement-3cr12-reaches-one-million-tonnes-milestone-2012-05-17.

ESAB (2011) *Technical handbook: Stainless steel welding*. Available at: http://assets.esab.com/asset-bank/assetfile/12295.pdf (Accessed: 29 February 2020).

European Committee for Standardisation (2011) *DIN EN ISO 148-1-Metallic materials – Charpy pendulum impact test*.

Folkhard, E. (1988) *Welding metallurgy of stainless steels*. New York: Springer-Verlag Wien.

Garth, S.W.F. and Lyttle, K. (2007) *7 effects of shielding gas, The Welder*. Available at: https://www.thefabricator.com/thewelder/article/arcwelding/7-effects-of-shielding-gas#:~:text=Shielding gases with greater reactivity, out-of-position control. (Accessed: 28 January 2022).

Hu, Shuai, Yaozong Mao, Xianbin Liu, En-hou Han, and Hannu Hänninen. (2020) 'Intergranular corrosion behaviour of low-chromium ferritic stainless steel without Cr-carbide precipitation after ageing', *Corrosion Science*, 166(December 2019), p. 108420. doi: 10.1016/j.corsci.2019.108420.

International Stainless-Steel Forum (2017) *Railcars in Stainless Steel: A Sustainable Solution for Sustainable Public Transport*. Available at: http://www.worldstainless.org/Files/ISSF/non-image-files/PDF/ISSF_Railcars_in_Stainless_Steel.pdf (Accessed: 11 October 2019).

International Stainless-Steel Forum (2018) *The Freight Industry, The Ferritic Solution, Ferritic Stainless-Steel Applications*. Available at: https://www.icdacr.com/download/TeamStainless-

TheFreightIndustry.pdf (Accessed: 4 October 2019).

Kah, P. and Martikainen, J. (2012) 'Influence of shielding gases in the welding of metals', *International Journal of Advanced Manufacturing Technology*, 64(9–12), pp. 1411–1421. Available at: https://www.researchgate.net/publication/257336726 Influence (Accessed: 16 October 2019).

Kapustka, N. (2012) *Arc Welding Capabilities at EWI*. Available at: https://docplayer.net/24086664-Arc-welding-capabilities-at-ewi.html (Accessed: 20 August 2020).

Khosla, Guy, Daniel Balint, Didier Farrugia, Matthew Hole, and Catrin M. Davies. (2018) 'Analysis of an as-cast high Si slab to elucidate fundamental causes of the fracture mechanism: Clinking', *Procedia Structural Integrity*, 13, pp. 1447–1452. doi: 10.1016/j.prostr.2018.12.300.

Kotecki, D. and Siewert, T. (1992) 'WRC-1992 constitution diagram for stainless steel weld metals: a modification of the WRC-1988 diagram', *Weld J*, 71(5), pp. 171–178. Available at: http://www.dacapo.com/filer/schaeffler_diagram.pdf.

Kotecki, D.J. (1993) *ASM Handbook: Volume 6, Welding, Brazing and Soldering*. ASM International.

Kou, S. (2003) *Welding Metallurgy*. New Jersey: John Wiley & Sons.

Lakshminarayanan, A.K. and Balasubramanian, V. (2012) 'Influences of welding processes on microstructure and mechanical properties of modified 12 wt. % Cr ferritic stainless steel', *International Journal of Manufacturing Research*, 7(4), pp. 331–353. doi:10.1504/IJMR.2012.050100.

Lakshminarayanan, A.K., Balasubramanian, V. and Madhusudhan Reddy, G. (2011) 'Microstructure and mechanical properties of electron beam-welded AISI 409M-grade ferritic stainless steel', *International Journal of Advanced Manufacturing Technology*, 55(1–4), pp. 153–162. doi:10.1007/s00170-010-3044-1.

Liao, M.T. and Chen, W.J. (1998) 'The effect of shielding-gas compositions on the microstructure and mechanical properties of stainless-steel weldments', *Materials Chemistry and Physics*, 55(2), pp. 145–151. doi:10.1016/S0254-0584(98)00134-5.

Lippold, J.C. and Kotecki, D.J. (2005) *Welding metallurgy and weldability of stainless steels*. John Wiley & Sons.

Luijan, J., Surin, P. and Wished, K. (2020) 'The Effect of Welding Parameters on Joining Dissimilar Low Carbon Steel and 3CR12 Ferritic Stainless Steel by GTAW with ER308L Filler Metal', *Journal of Physics: Conference Series*, 1519(1). doi:10.1088/1742-6596/1519/1/012010.

Madyira, D.M., Kaymakci, A. and Nkwanyana, N. (2019) 'The Effect of Metal Transfer Modes on Mechanical Properties of 3CR12 Stainless Steel', *Transactions of the Canadian Society for Mechanical Engineering*, 44(Number 2). doi: https://doi.org/10.1139/tcsme-2018-0125.

Mathison, J. (2008) *Understanding transfer modes for GMAW, The Welder*. Available at: https://www.thefabricator.com/thewelder/article/consumables/understanding-transfer-modes-for-gmaw (Accessed: 1 February 2022).

Mvola, B. and Kah, P. (2016) ‘Effects of shielding gas control: welded joint properties in GMAW process optimization’, *The International Journal of Advanced Manufacturing Technology* [Preprint]. doi:10.1007/s00170-016-8936-2.

Panmongkol, P. and Phung-on, I. (2021) ‘Effect of backing gas mixtures on corrosion properties of stainless-steel grade 304 weld metal by autogenous GTAW *’, *Journal of Materials Research and Technology*, 11, pp. 1559–1570. doi: 10.1016/j.jmrt.2021.01.125.

Quintino, L., Liskevich, O. and Vilarinho, L. (2013) ‘Heat input in full penetration welds in gas metal arc welding (GMAW)’, *International Journal of Advanced Manufacturing Technology*, 68(9–12), pp. 2833–2840. doi:10.1007/s00170-013-4862-8.

Rao, Z.H., Hu, J., and Liao, S.M. (2009) ‘Study the shielding gas effects on transport phenomena in GMAW arc’, *20th International Symposium on Transport Phenomena (ISTP20)* [Preprint], (July). Available at: https://www.researchgate.net/publication/259870175_Study_the_shielding_gas_effects_on_transport_phenomena_in_GMAW_arc/stats (Accessed: 29 January 2022).

Rhee, S. and Kannatey-Asibu, E. (1992) ‘Observation of Metal Transfer during Gas Metal Arc Welding’, *Welding Journal*, 10, pp. 381–387. Available at: https://app.aws.org/wj/supplement/WJ_1992_10_s381.pdf (Accessed: 31 January 2022).

S. Azar, A. and Diplas, S. (2022) ‘Fundamental aspects of processing multi-metallic components using additive manufacturing technologies’, *European Journal of Materials*, 2(1), pp. 234–364. doi:10.1080/26889277.2022.2073568.

Schweighardt, F. (2007) *Choosing shielding gases for arc welding*, *The Fabricator*. Available at: https://www.thefabricator.com/thefabricator/article/consumables/choosing-shielding-gases-for-arc-welding (Accessed: 11 February 2020).

Taban, E., Deleu, E. and Dhooge, A. (2008) ‘Evaluation of dissimilar welds between ferritic stainless steel modified 12% Cr and carbon steel S355’, *Welding Journal (Miami, Fla)*, 87(12), pp. 291–297. Available at: https://www.researchgate.net/publication/285963241 (Accessed: 1 October 2019).

Taban, E., Deleu, E. and Dhooge, A. (2012) ‘Effect of the consumable on the properties of gas metal arc welded EN 1.4003-type stainless steel’, *Welding Journal*, 91(8), pp. 213–221. Available at: https://www.researchgate.net/publication/285963088 (Accessed: 1 October 2019).

Taylor, P., Filho, D.F. and Ferraresi, V.A. (2010) ‘The influence of gas shielding composition and contact tip to work distance in short circuit metal transfer of ferritic stainless steel’, *Welding International*, 24(November 2014), pp. 206–213. doi:10.1080/09507110902843842.

The Lincoln Electric Company (2014) *Welding Guide (Gas Metal Arc Welding)*. Available at: https://m.lincolnelectric.com/assets/global/Products/Consumable_MIGGMAWWires-SuperArc-SuperArcLA-90/c4200.pdf (Accessed: 14 November 2019).

Du Toit, M., Van Rooyen, G.T. and Smith, D. (2010) ‘Heat-Affected Zone Sensitization and Stress Corrosion Cracking in 12% Chromium Type 1.4003 Ferritic Stainless Steel’, *The Welding World*, 63(5), pp. 395–404. Available at: https://www.researchgate.net/publication/250394975 (Accessed: 1 October 2019).

Valiente Bermejo, M.A., Karlsson, L. and Svensson, L.E. (2015) 'Effect of shielding gas on welding performance and properties of duplex and super duplex stainless steel welds', *Welding in the World*, 59(2), pp. 239–249. doi:10.1007/s40194-014-0199-7.

Zhao, Sipei, Xiaojun Qiu, Ian Burnett, Malcolm Rigby, and Anthony Lele. (2019) 'GMAW metal transfer mode identification from welding sound', *Australian Acoustical Society Annual Conference, AAS 2018*, (June), pp. 482–491. Available at: https://www.researchgate.net/publication/341900282_GMAW_metal_transfer_mode_identification_from_welding_sound (Accessed: 11 July 2022).